

UNCLASSIFIED

SECURITY CLASSIFICATION OF THIS PAGE (When Data Entered)

A056695

REPORT DOCUMENTATION PAGE		READ INSTRUCTIONS BEFORE COMPLETING FORM
1. REPORT NUMBER TR-3808	2. GOVT ACCESSION NO.	3. RECIPIENT'S CATALOG NUMBER
4. TITLE (and Subtitle) NONLINEAR ROLLING MOTION ANALYSIS OF A CANARD-CONTROLLED MISSILE CONFIGURATION AT ANGLES OF ATTACK FROM 0 TO 30° IN INCOMPRESSIBLE FLOW		5. TYPE OF REPORT & PERIOD COVERED Final FY77
		6. PERFORMING ORG. REPORT NUMBER
7. AUTHOR(s) Samuel R. Hardy		8. CONTRACT OR GRANT NUMBER(s)
9. PERFORMING ORGANIZATION NAME AND ADDRESS Naval Surface Weapons Center ATTN: Code K21 Dahlgren, Virginia 22448		10. PROGRAM ELEMENT, PROJECT, TASK AREA & WORK UNIT NUMBERS NIF: CA82EBACE
11. CONTROLLING OFFICE NAME AND ADDRESS Naval Weapons Center China Lake, California 93555		12. REPORT DATE May 1978
		13. NUMBER OF PAGES 70
14. MONITORING AGENCY NAME & ADDRESS (if different from Controlling Office)		15. SECURITY CLASS. (of this report) UNCLASSIFIED
		15a. DECLASSIFICATION/DOWNGRADING SCHEDULE
16. DISTRIBUTION STATEMENT (of this Report) Approved for public release; distribution unlimited.		
17. DISTRIBUTION STATEMENT (of the abstract entered in Block 20, if different from Report) Approved for public release; distribution unlimited.		
18. SUPPLEMENTARY NOTES		
19. KEY WORDS (Continue on reverse side if necessary and identify by block number) rolling motion, finned missile canard-controlled missile roll damping dynamic wind tunnel test		
20. ABSTRACT (Continue on reverse side if necessary and identify by block number) Dynamic subsonic wind tunnel test data are presented for four canard-controlled missile configurations at angles of attack from 0 to 30°. The configurations included three body build-up configurations (canard plus body, body plus tail, and canard plus body plus tail) with zero fin deflections. A canard plus body plus tail configuration with a 15° canard pitch control deflection was also tested. Nonlinear static and dynamic roll moment coefficients were extracted from the test data by fitting a differen-		

DD FORM 1 JAN 73 1473

EDITION OF 1 NOV 68 IS OBSOLETE
S/N 0102-014-6801

UNCLASSIFIED

SECURITY CLASSIFICATION OF THIS PAGE (When Data Entered)

78 07 24 001

UNCLASSIFIED

SECURITY CLASSIFICATION OF THIS PAGE(When Data Entered)

20. (Continued)

tial equation of rolling motion to the test data using a "global" nonlinear least-squares procedure.

The results indicated that the equation of motion was adequate to describe the canard-controlled configurations' rolling motion. Extracted linear roll damping coefficients showed that the roll damping moment is a nonlinear function of angle of attack for all the configurations. Roll damping was also found to vary with the missiles' roll angle at angles of attack above 20° . The results for the body build-up configurations show that there is a significant canard/tail interference present on the canard plus body plus tail configuration. The canard contribution to the induced roll moment is small. The results for the canard plus body plus tail configuration with the 15° pitch control deflection on the canards show that the canard deflection generally increases the roll damping moment.

UNCLASSIFIED

SECURITY CLASSIFICATION OF THIS PAGE(When Data Entered)

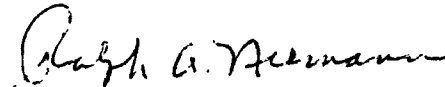
FOREWORD

This technical report documents dynamic wind tunnel test data and the extraction of nonlinear dynamic roll moment coefficients from these data. The test and analysis were conducted under a program to investigate the rolling motion of cruciform canard-controlled missiles at moderate angles of attack.

The work was supported by the Naval Air Systems Command (Mr. W. C. Volz, AIR-320C) under AIRTASK A03W-350D/004B-6F32-300-000.

This report has been reviewed for technical accuracy and approved by Mr. Peter Daniels, Aeromechanics Branch; Dr. Frankie G. Moore, Head, Aeromechanics Branch; and Mr. Herman Caster, Head, Exterior Ballistics Division of the Strategic Systems Department.

Released by:



R. A. NIEMANN, Head
Strategic Systems Department

CONTENTS

	<u>Page</u>
INTRODUCTION	1
WIND TUNNEL TEST DATA	2
ROLL MOMENT COEFFICIENTS	4
SUMMARY AND RECOMMENDATIONS	16
REFERENCES	18

APPENDIXES

A--OBSERVED ROLL ANGLE VERSUS FRAME NUMBER FOR CANARD-CONTROLLED MISSILE CONFIGURATIONS AT ANGLES OF ATTACK FROM 0 TO 30°

B--COMPARISON PLOTS OF COMPUTED AND OBSERVED ROLL ANGLE VERSUS TIME FOR THE CANARD-CONTROLLED MISSILE CONFIGURATIONS AT ANGLES OF ATTACK FROM 0 TO 30°

C--NOMENCLATURE

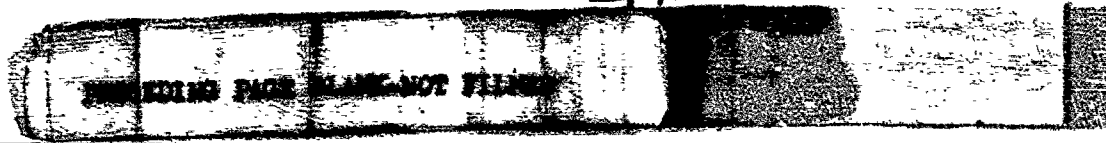
DISTRIBUTION

SI Conversion

<u>Multiply</u>	<u>By</u>	<u>To Obtain</u>
inch	2.54	centimeter
degree	0.01745	radian
foot/second	0.3048	metre/second
foot	0.3048	metre
pound-force/foot ²	47.88	pascal

Accession	15
BY	
DISTRIBUTION/AVAILABILITY CODES	
Dist	AVAIL. CODES SPECIAL
A	

v



LIST OF ILLUSTRATIONS

<u>Figure</u>		<u>Page</u>
1	Canard-Controlled Missile Configurations	3
2	Extracted Linear Roll Damping Moment Coefficient Derivative Versus Angle of Attack for Canard-Controlled Missile Configurations	7
3	Experimental Canard/Tail Interference Versus Angle of Attack for the Canard Plus Body Plus Tail Configuration ($\delta = 0^\circ$) . . .	8
4	Comparison of Experimental and Estimated Linear Roll Damping Moment Coefficient Derivative Versus Angle of Attack for Canard Plus Body Plus Tail Configuration ($\delta = 0^\circ$)	9
5	Estimated Canard/Tail Interference Versus Angle of Attack for the Canard Plus Body Plus Tail Configuration ($\delta = 0^\circ$)	9
6	Linear Roll Damping Moment Coefficient Derivative Variation with Roll Angle Versus Angle of Attack for the Canard- Controlled Missile Configurations	10
7	Total Roll Damping Moment Coefficient Versus Roll Angle for the Body Plus Tail Configuration at a 25° Angle of Attack . . .	11
8	Rolling Motion Phase Plane for Body Plus Tail Configuration at a 25° Angle of Attack	12
9	Extracted Induced Roll Moment Coefficient Versus Angle of Attack for Canard-Controlled Missile Configurations	13
10	Roll Trim Angle Due to the Induced Roll Moment	14
11	Extracted Fin Cant Roll Moment Coefficients Versus Angle of Attack for Canard-Controlled Missile Configurations	15
12	Extracted Mass/Aerodynamic Roll Moment Asymmetry Coefficients Versus Angle of Attack for Canard-Controlled Missile Configurations	15
A-1	Observed Roll Angle Versus Frame Number at a 0° Angle of Attack for Run 24	A-1
A-2	Observed Roll Angle Versus Frame Number at a 5° Angle of Attack for Run 25	A-1
A-3	Observed Roll Angle Versus Frame Number at a 10° Angle of Attack for Run 26	A-2
A-4	Observed Roll Angle Versus Frame Number at a 15° Angle of Attack for Run 27	A-2
A-5	Observed Roll Angle Versus Frame Number at a 20° Angle of Attack for Run 28	A-3
A-6	Observed Roll Angle Versus Frame Number at a 25° Angle of Attack for Run 29	A-3
A-7	Observed Roll Angle Versus Frame Number at a 30° Angle of Attack for Run 30	A-4
A-8	Observed Roll Angle Versus Frame Number at a 0° Angle of Attack for Run 347	A-4
A-9	Observed Roll Angle Versus Frame Number at a 5° Angle of Attack for Run 348	A-5
A-10	Observed Roll Angle Versus Frame Number at a 10° Angle of Attack for Run 349	A-5

LIST OF ILLUSTRATIONS (Continued)

<u>Figure</u>		<u>Page</u>
A-11	Observed Roll Angle Versus Frame Number at a 15° Angle of Attack for Run 350	A-6
A-12	Observed Roll Angle Versus Frame Number at a 20° Angle of Attack for Run 351	A-6
A-13	Observed Roll Angle Versus Frame Number at a 25° Angle of Attack for Run 352	A-7
A-14	Observed Roll Angle Versus Frame Number at a 30° Angle of Attack for Run 353	A-7
A-15	Observed Roll Angle Versus Frame Number at a 0° Angle of Attack for Run 262	A-8
A-16	Observed Roll Angle Versus Frame Number at a 5° Angle of Attack for Run 263	A-8
A-17	Observed Roll Angle Versus Frame Number at a 10° Angle of Attack for Run 264	A-9
A-18	Observed Roll Angle Versus Frame Number at a 15° Angle of Attack for Run 265	A-9
A-19	Observed Roll Angle Versus Frame Number at a 20° Angle of Attack for Run 266	A-10
A-20	Observed Roll Angle Versus Frame Number at a 25° Angle of Attack for Run 267	A-10
A-21	Observed Roll Angle Versus Frame Number at a 30° Angle of Attack for Run 268	A-11
A-22	Observed Roll Angle Versus Frame Number at a 0° Angle of Attack for Run 283	A-11
A-23	Observed Roll Angle Versus Frame Number at a 5° Angle of Attack for Run 284	A-12
A-24	Observed Roll Angle Versus Frame Number at a 10° Angle of Attack for Run 285	A-12
A-25	Observed Roll Angle Versus Frame Number at a 15° Angle of Attack for Run 286	A-13
A-26	Observed Roll Angle Versus Frame Number at a 20° Angle of Attack for Run 287	A-13
A-27	Observed Roll Angle Versus Frame Number at a 25° Angle of Attack for Run 288	A-14
A-28	Observed Roll Angle Versus Frame Number at a 30° Angle of Attack for Run 289	A-14
B-1	Comparison of Observed and Computed Roll Angles at a 0° Angle of Attack for Run 24	B-1
B-2	Comparison of Observed and Computed Roll Angles at a 5° Angle of Attack for Run 25	B-1
B-3	Comparison of Observed and Computed Roll Angles at a 10° Angle of Attack for Run 26	B-2
B-4	Comparison of Observed and Computed Roll Angles at a 15° Angle of Attack for Run 27	B-2
B-5	Comparison of Observed and Computed Roll Angles at a 20° Angle of Attack for Run 28	B-3

LIST OF ILLUSTRATIONS (Continued)

<u>Figure</u>		<u>Page</u>
B-6	Comparison of Observed and Computed Roll Angles at a 25° Angle of Attack for Run 29	B-3
B-7	Comparison of Observed and Computed Roll Angles at a 30° Angle of Attack for Run 30	B-4
B-8	Comparison of Observed and Computed Roll Angles at a 0° Angle of Attack for Run 347	B-4
B-9	Comparison of Observed and Computed Roll Angles at a 5° Angle of Attack for Run 348	B-5
B-10	Comparison of Observed and Computed Roll Angles at a 10° Angle of Attack for Run 349	B-5
B-11	Comparison of Observed and Computed Roll Angles at a 15° Angle of Attack for Run 350	B-6
B-12	Comparison of Observed and Computed Roll Angles at a 20° Angle of Attack for Run 351	B-6
B-13	Comparison of Observed and Computed Roll Angles at a 25° Angle of Attack for Run 352	B-7
B-14	Comparison of Observed and Computed Roll Angles at a 30° Angle of Attack for Run 353	B-7
B-15	Comparison of Observed and Computed Roll Angles at a 0° Angle of Attack for Run 262	B-8
B-16	Comparison of Observed and Computed Roll Angles at a 5° Angle of Attack for Run 263	B-8
B-17	Comparison of Observed and Computed Roll Angles at a 10° Angle of Attack for Run 264	B-9
B-18	Comparison of Observed and Computed Roll Angles at a 15° Angle of Attack for Run 265	B-9
B-19	Comparison of Observed and Computed Roll Angles at a 20° Angle of Attack for Run 266	B-10
B-20	Comparison of Observed and Computed Roll Angles at a 25° Angle of Attack for Run 267	B-10
B-21	Comparison of Observed and Computed Roll Angles at a 30° Angle of Attack for Run 268	B-11
B-22	Comparison of Observed and Computed Roll Angles at a 0° Angle of Attack for Run 283	B-11
B-23	Comparison of Observed and Computed Roll Angles at a 5° Angle of Attack for Run 284	B-12
B-24	Comparison of Observed and Computed Roll Angles at a 10° Angle of Attack for Run 285	B-12
B-25	Comparison of Observed and Computed Roll Angles at a 15° Angle of Attack for Run 286	B-13
B-26	Comparison of Observed and Computed Roll Angles at a 20° Angle of Attack for Run 287	B-13
B-27	Comparison of Observed and Computed Roll Angles at a 25° Angle of Attack for Run 288	B-14
B-28	Comparison of Observed and Computed Roll Angles at a 30° Angle of Attack for Run 289	B-14

INTRODUCTION

This work is part of a joint program with the Naval Weapons Center (NWC), China Lake, California, to improve the methods of predicting the rolling motion of non-roll-controlled guided missiles. Guided missiles, whether roll controlled or not, that are flown to high angles of attack encounter large variations in aerodynamic roll moment. An effective design requires analysis and prediction of rolling motion phenomena. This work was conducted to provide further insight into the roll characteristics of canard-controlled missiles at high angles of attack.

The specific objective of the Naval Surface Weapons Center (NSWC), Dahlgren, Virginia, was to provide experimental dynamic roll moment coefficients (roll damping) for a cruciform, canard-controlled missile. The experimental data are to be used by NWC to evaluate NWC-sponsored prediction techniques of roll damping characteristics for canard missiles. This experimental data will serve as a data base for comparison with "theory."

NSWC had previously developed a fitting technique to extract nonlinear roll moment coefficients from single degree-of-freedom rolling motion data. The basis of this procedure is a nonlinear differential equation of rolling motion, first set forth by Daniels.^{1*} The equation of motion describes the roll phenomena ("linear" rolling motion, roll "slowdown," roll "lockin," "breakout," and "speedup") of a cruciform-finned (body plus tail) missile at angles of attack from 0 to 90°. The roll moment coefficients are extracted from observed roll angular data using a "global" nonlinear least-squares fitting procedure developed by Cohen and Clare.² The procedure was used successfully by Cohen, Clare, and Stevens³ to determine roll moment coefficients for a cruciform body plus tail configuration (Basic Finner) at high angles of attack. It seemed logical to extend the fitting procedures to the canard-

*Raised numerals refer to identically numbered references listed at the end of the text.

controlled configuration, even though the equation of motion was not specifically developed for guided missile configurations with control deflections.

This report presents rolling motion data and extracted roll moment coefficients for four canard-controlled missile configurations at angles of attack from 0 to 30° at subsonic speed.

WIND TUNNEL TEST DATA

The canard-controlled missile model used in the wind tunnel tests was a 10-caliber, tangent ogive-cylinder body. The canards and tail were detachable so that body build-up configurations could be tested. The configurations discussed in this report include three body build-up configurations (canard plus body, body plus tail, and canard plus body plus tail) that have zero canard and tail deflections ($\delta = 0^\circ$). The fourth configuration was a canard plus body plus tail configuration with two opposing canards deflected 15° ($\delta_c = 15^\circ$) to simulate a pitch maneuver. Canard and tail deflections were fixed during test runs. Figure 1 shows diagrams of the four canard-controlled missile configurations.

The wind tunnel tests⁴ were conducted in the 7x10-ft low-speed wind tunnel of the Army Air Mobility Research and Development Laboratory, Moffett Field, California. The free-stream velocity was about 113 ft/sec. The dynamic pressure during the test was approximately 15 lb/ft² with a Reynolds number of approximately 6.6×10^5 /ft. The model was mounted on an air bearing so that it was free to roll. Angle of attack was constant during test runs.

Measurements of roll angle (γ) as a function of time were recorded using a high-speed motion picture camera. The film was digitized to obtain roll angle. Appendix A shows the resulting plots of roll angle versus film frame

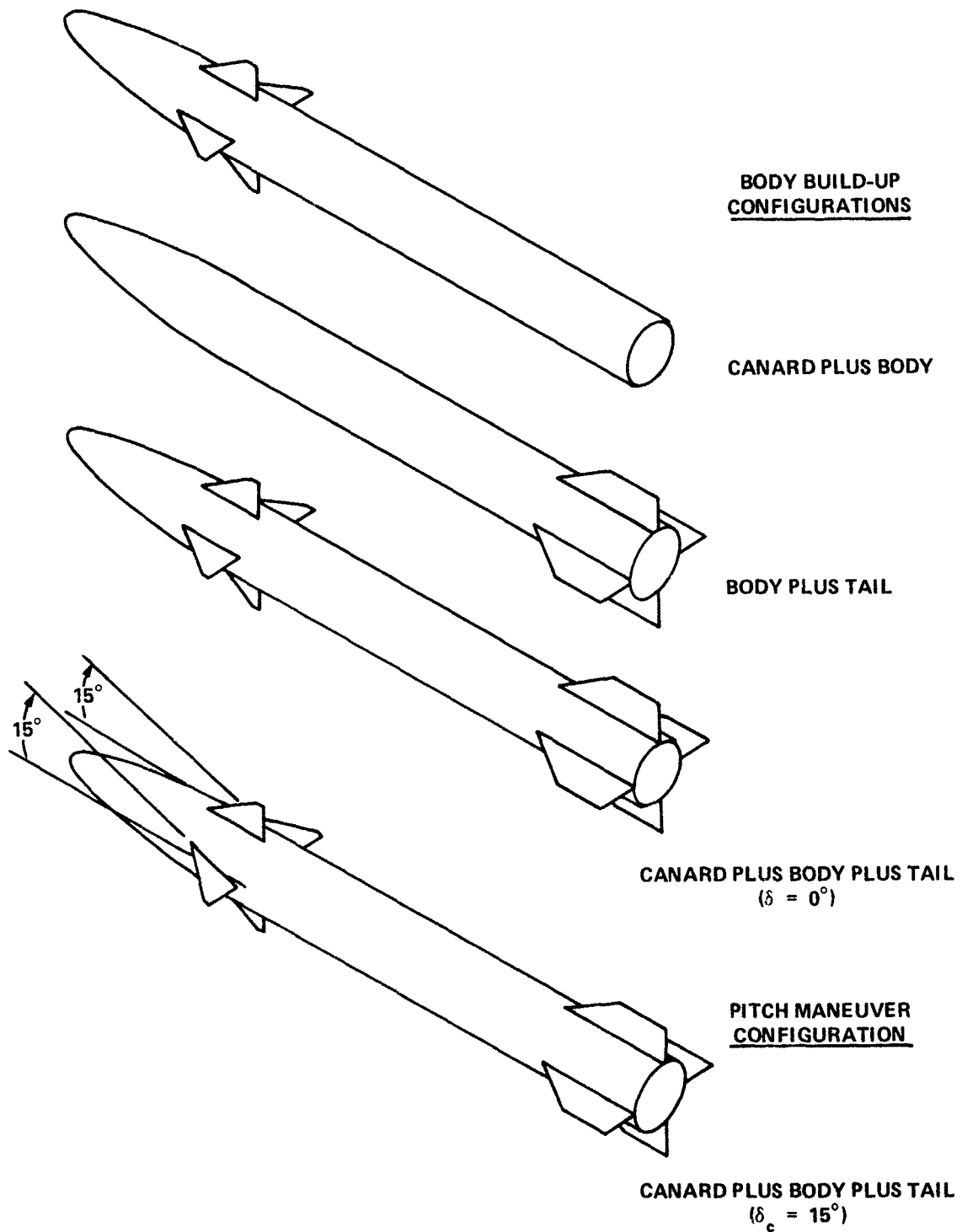


Figure 1. Canard-Controlled Missile Configurations

In the preliminary analysis of the canard plus body plus tail with zero fin deflections, only five basic (first order) coefficients were extracted.⁴ These roll moment coefficients included fin cant ($C_{\ell\delta}$), linear roll damping derivative ($C_{\ell p}$), induced roll moment ($C_{\ell(4\gamma)}$), and two asymmetry terms (C_{ac} and C_{as}). These coefficients were thought to be adequate to model the rolling motion; however, subsequent analysis of the rolling motion of the configurations at angles of attack from 20 to 30° showed that an additional coefficient was needed to explain the roll oscillatory motion. The linear roll damping derivative coefficient variation with roll angle ($C_{\ell p(4\gamma)}$) was introduced to account for the rolling motion oscillations that do not damp. (Higher order roll damping variation with roll rate ($C_{\ell p^3}$) was extracted from several runs; however, the results appeared to be incorrect and data fits were not significantly improved.) The linear roll damping derivative coefficient variation with roll angle ($C_{\ell p(4\gamma)}$) was extracted only when the data fits were significantly improved.

Appendix B presents comparison plots of observed and computed roll angle versus time. The plots show the results of the data fits. The observed data, roll angle versus time, were obtained from the roll angle versus frame number data in Appendix A by correlating frame number to time. The computed data were calculated using Equation (1) and the set of roll moment coefficients extracted for that configuration at that particular angle of attack. The small lines drawn normal to the computed lines indicate segment locations used in the fitting process. The computed data matches the observed data well.

These comparisons indicate that Equation (1) is an adequate model for determining the roll moment coefficients for a canard-controlled missile at moderate angles of attack, and the good agreement is considered to be validation of the extracted roll moment coefficients.

The linear roll damping moment coefficient derivative ($C_{\ell p}$) results are presented in Figure 2. $C_{\ell p}$ is nonlinear with respect to angle of attack for all of the configurations. The values of $C_{\ell p}$, noted by darkened data points in

Table 1. Aerodynamic Roll Moment Coefficient Correlation*

Coefficient		Description
Conventional Nomenclature	Computer Program Nomenclature	
$C_{l\delta}$	C_{00}	Fin cant roll moment coefficient
$C_{l\delta(4\gamma)}$	C_{01}	Variation of fin cant moment Coefficient with roll angle
$C_{l\delta(8\gamma)}$	C_{02}	
$C_{l\delta(12\gamma)}$	C_{03}	
\vdots	\vdots	
$C_{l\delta(4K\gamma)}$	C_{0K}	
C_{lp}	C_{10}	Linear roll damping moment coefficient derivative
C_{lp^2}	C_{20}	Quadratic roll damping moment coefficient derivative
C_{lp^3}	C_{30}	Cubic roll damping moment coefficient derivative
\vdots	\vdots	
C_{lp^J}	C_{J0}	
$C_{lp(4\gamma)}$	C_{11}	Variation of linear roll damping moment coefficient derivative with roll angle
$C_{lp(8\gamma)}$	C_{12}	
$C_{lp(12\gamma)}$	C_{13}	
\vdots	\vdots	
$C_{lp(4K\gamma)}$	C_{1K}	
$C_{l(4\gamma)}$	S_{01}	Induced rolling moment coefficients
$C_{l(8\gamma)}$	S_{02}	
$C_{l(12\gamma)}$	S_{03}	
\vdots	\vdots	
$C_{l(4K\gamma)}$	S_{0K}	
	C_{ac}	Roll asymmetry coefficients (Combinations of aerodynamic and mass asymmetry constants)
	C_{as}	

*All coefficients are a function of the missile's angle of attack.

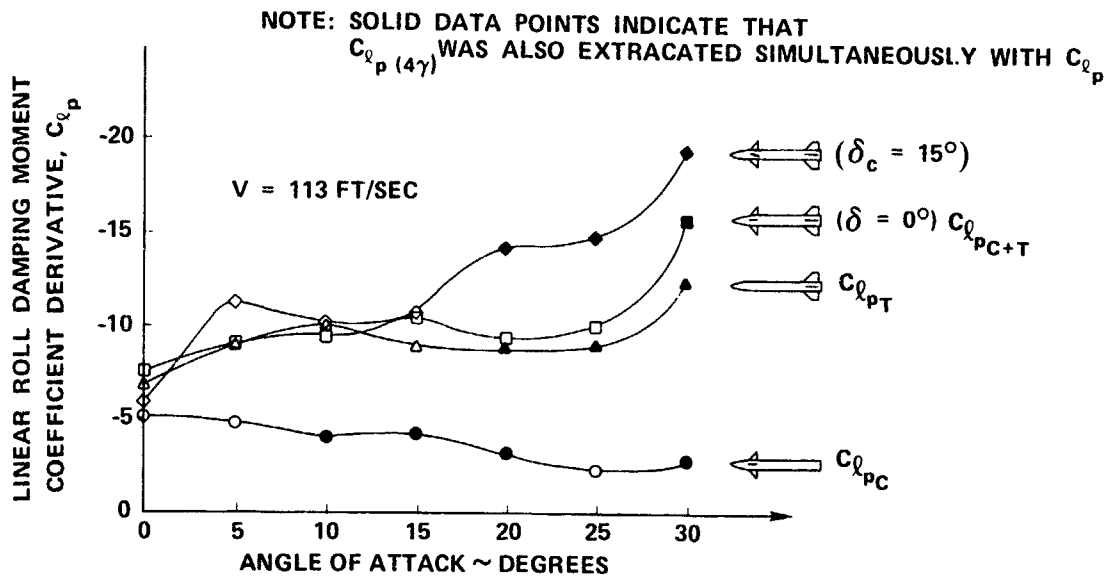


Figure 2. Extracted Linear Roll Damping Moment Coefficient Derivative Versus Angle of Attack for Canard-Controlled Missile Configurations

Figure 2, indicate that $C_{\ell_p(4\gamma)}$ was also extracted simultaneously with C_{ℓ_p} . C_{ℓ_p} alone was found to be insufficient to model roll damping moments for those configurations at those angles of attack. Figure 2 shows that the C_{ℓ_p} of the canard plus body configuration is smaller than the C_{ℓ_p} of the body plus tail configuration over the angle of attack range. C_{ℓ_p} was referenced to the model body diameter and the canards are smaller than the tail fins. The C_{ℓ_p} of the body plus tail and the canard plus body plus tail configurations are nearly the same over the angle of attack range. In addition, Figure 2 also shows that the 15° canard pitch control deflections make C_{ℓ_p} more negative at angles of attack above 15° .

Figure 3 shows that there is significant canard/tail interference present on the canard plus body plus tail configuration especially at lower angles of attack. The interference nearly cancels the canard contribution. Figure 4 shows a comparison plot of the extracted experimental and estimated C_{l_p} values for the canard plus body plus tail configuration. The estimated values⁸ show good agreement with the experimental data except at a 30° angle of attack. However, estimates of the canard/tail interference shown in Figure 5 do not agree with the experimental interference shown in Figure 3.

Examination of the values obtained for $C_{l_p(4\gamma)}$ in Figure 6 shows that opposite trends are observed in this coefficient for the configurations with and without a tail. These trends are obvious in the rolling motion data, Appendix A. When the canard plus body configuration (without a tail) is circulating, the average roll damping moment is smaller at all angles of attack than the configurations with a tail. This is evident in the rolling motion plots, since it requires more revolutions for the canard plus body to

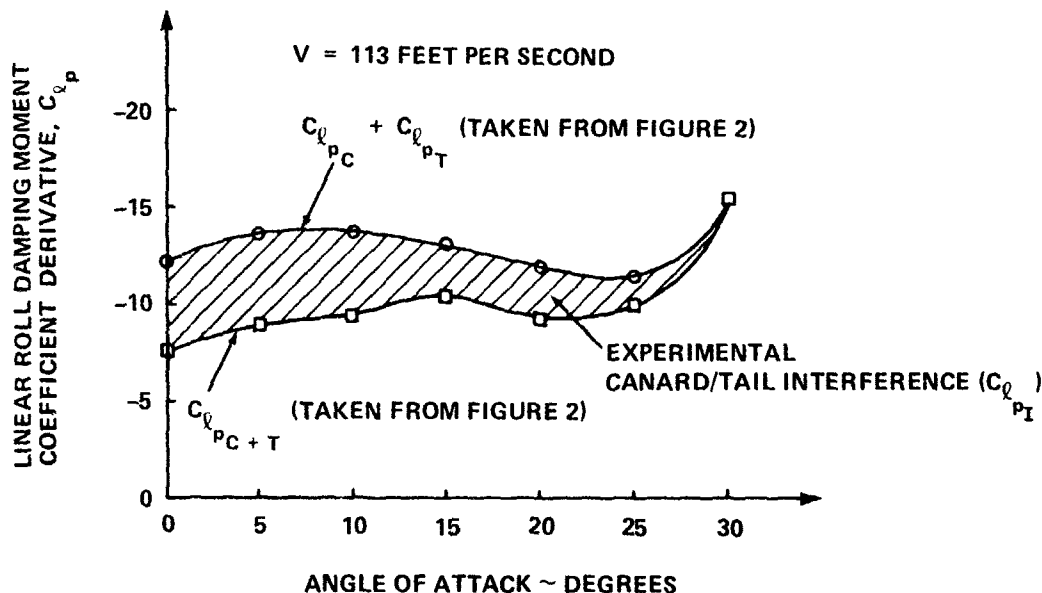
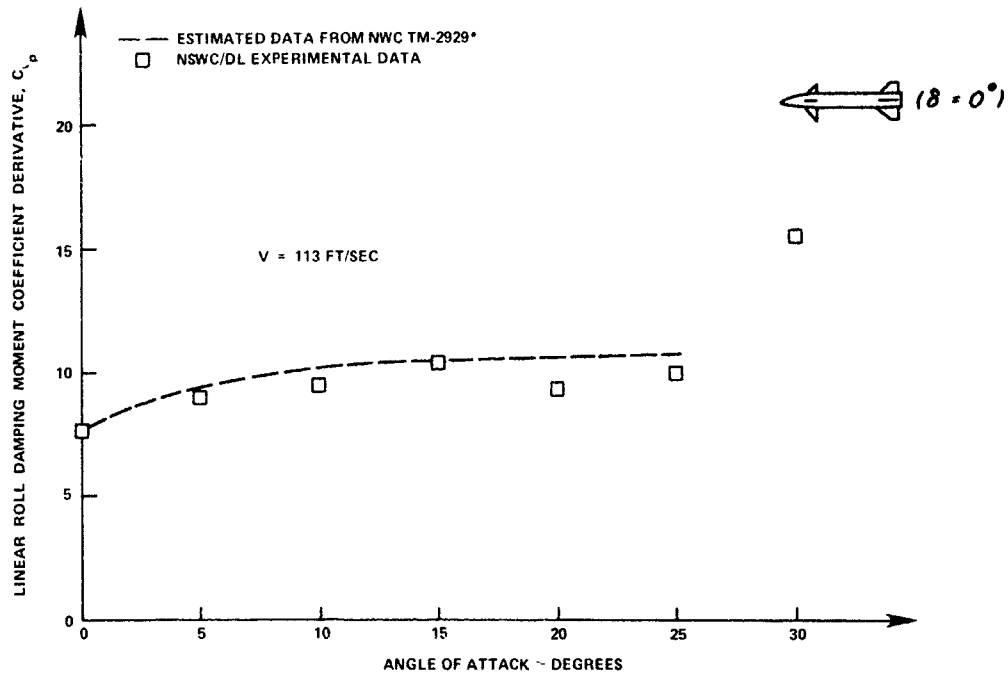
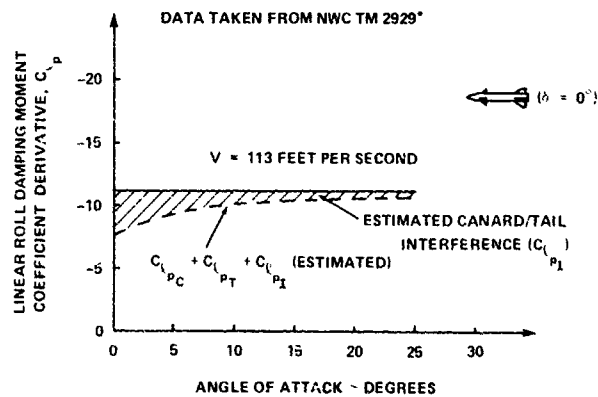


Figure 3. Experimental Canard/Tail Interference Versus Angle of Attack for the Canard Plus Body Plus Tail Configuration ($\delta = 0^\circ$)



*Meeker, R E Roll Damping Studies Progress Report For FY 1976 and 1976 TO NWC Technical Memorandum 2929, Naval Weapons Center, China Lake, California, October 1976

Figure 4. Comparison of Experimental and Estimated Linear Roll Damping Moment Coefficient Derivative Versus Angle of Attack for Canard Plus Body Plus Tail Configuration ($\delta = 0^\circ$)



*MEEKER R E ROLL DAMPING STUDIES PROGRESS REPORT FOR FY 1976 AND 1977 TO, NWC TECHNICAL MEMORANDUM 2929, NAVAL WEAPONS CENTER CHINA LAKE CALIFORNIA, OCTOBER 1976

Figure 5. Estimated Canard/Tail Interference Versus Angle of Attack for the Canard Plus Body Plus Tail Configuration ($\delta = 0^\circ$)

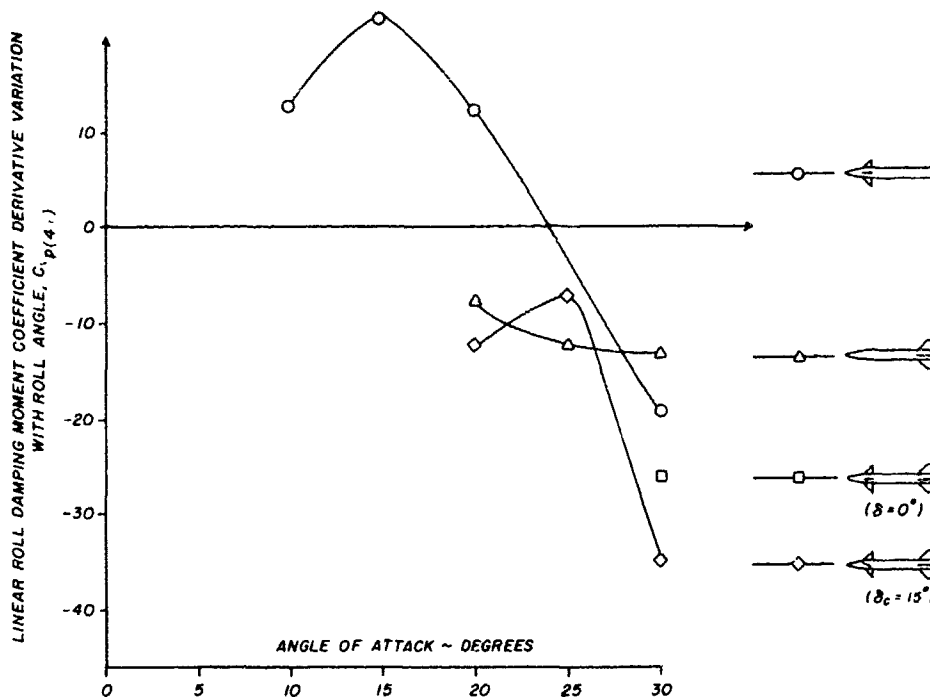


Figure 6. Linear Roll Damping Moment Coefficient Derivative Variation with Roll Angle Versus Angle of Attack for the Canard-Controlled Missile Configurations

damp. However, after the canard plus body configuration begins an oscillatory motion ("lockin"), the number of cycles to damp to a roll trim angle is smaller than for the configurations with a tail. This indicates the presence of strong negative damping moments in roll angle (γ) regions near the "lockin" roll trim angle and implies that $C_{l_p(4\gamma)}$ must be of the same sign as the induced roll moment coefficient for the canard plus body configuration. The extracted values for $C_{l_p(4\gamma)}$ and $C_{l(4\gamma)}$ show this result.

The roll angular data for the configurations with tails exhibit oscillatory motion at angles of attack from 20 to 30° that does not damp to a roll trim angle, but oscillates about that roll trim position. Because the roll oscillations do not damp, there must be a region of positive roll damping moment near the roll trim angle. For configurations with a tail, the sign of $C_{l_p(4\gamma)}$ must be opposite the sign of $C_{l(4\gamma)}$. To exhibit undamped oscillations,

the configurations with a tail must have $C_{l_p(4\gamma)}$ negative and larger than C_{l_p} for the particular angle of attack. This result can be shown by the superposition of average linear roll damping moment and the variation of the roll damping moment with roll angle, Figure 7.

The roll angular data for the body plus tail configuration at a 25° angle of attack, Figure B-13, and for the canard plus body plus tail ($\delta_c = 15^\circ$) at a 20° angle of attack, Figure B-26, show a gap in the computed data where the roll oscillatory data shifts from one roll trim angle to another. This cannot be predicted by the equation of motion. However, both data runs exhibit roll asymmetry and the extracted values of $C_{l_p(4\gamma)}$ show a region in γ where the damping moment is nearly zero. The zero damping region appears to be near a saddle point in the γ versus $\dot{\gamma}$ phase plane, Figure 8. Because the damping is zero near the saddle point and a roll asymmetry is present, it is possible that any small disturbance or unmodeled transient could cause

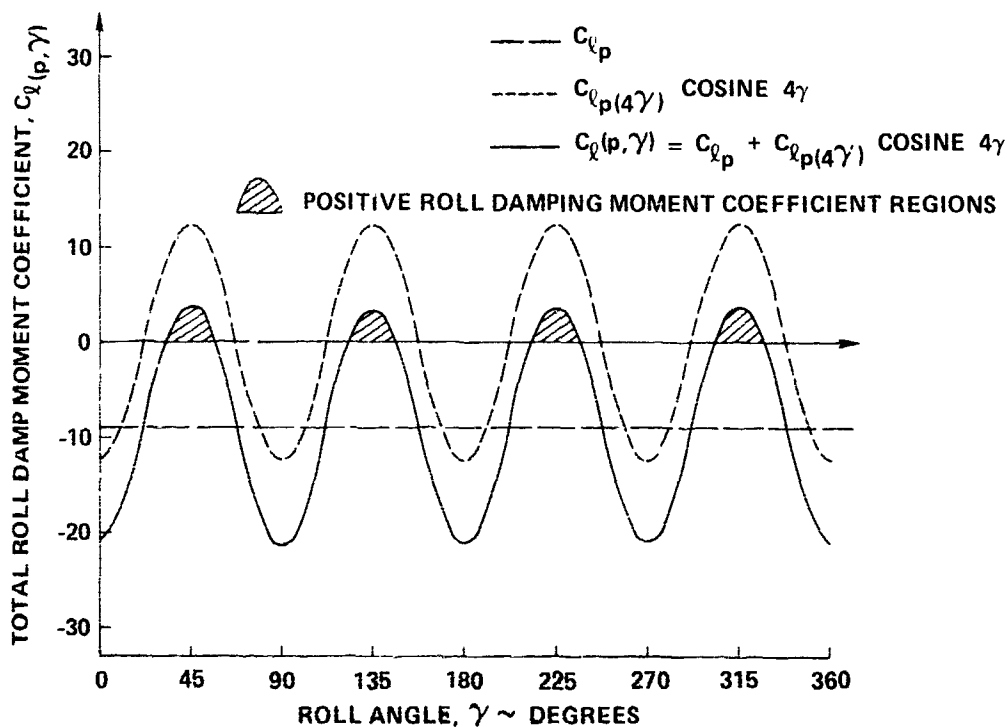


Figure 7. Total Roll Damping Moment Coefficient Versus Roll Angle for the Body Plus Tail Configuration at a 25° Angle of Attack

RUN 352 ALPHA = 25.0 DEG.

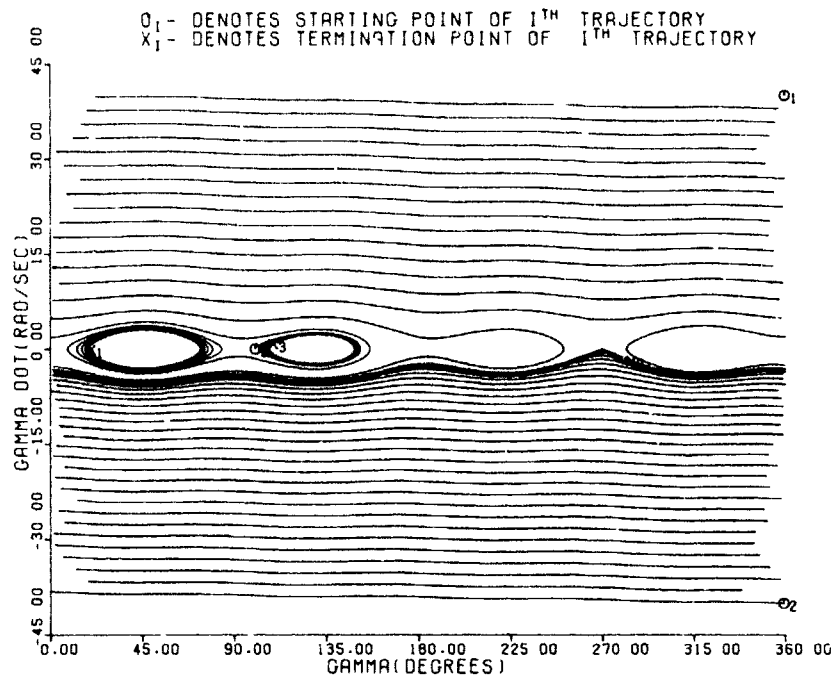


Figure 8. Rolling Motion Phase Plane for Body Plus Tail Configuration at a 25° Angle of Attack

the model to jump from oscillations about one roll trim angle to oscillations about one roll trim angle to oscillations about another adjacent roll trim angle. From Figure 8, it is possible for the motion to jump from Trajectory 1 to Trajectory 3, even though the jump is not modeled. Note that the phase plane was computed using extracted roll moment coefficients. The gap in the data does not effect the extracted coefficients since the observed roll data was segmented around the gap.

Figure 9 presents plots of the extracted induced roll moment coefficients ($C_{l(4\gamma)}$) as a function of angle of attack for the canard-controlled missile configurations. It should be noted that $C_{l(8\gamma)}$ was also extracted for the canard plus body plus tail configuration ($\delta = 0^\circ$) at a 25° angle of attack. The $C_{l(8\gamma)}$ was extracted because, in this instance, the fit was improved sig-

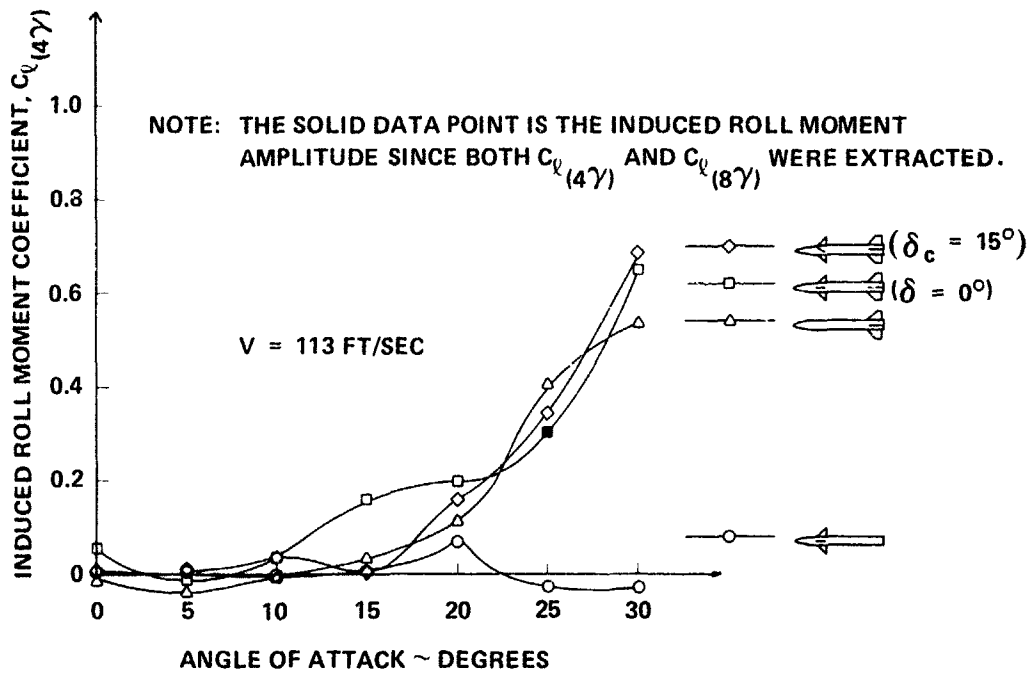
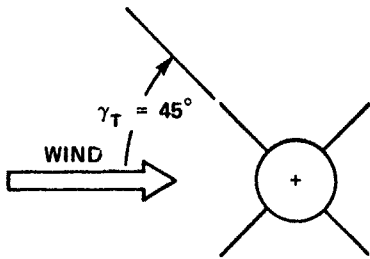


Figure 9. Extracted Induced Roll Moment Coefficient Versus Angle of Attack for Canard-Controlled Missile Configurations

nificantly. The total induced roll moment coefficient amplitude was plotted for this special case in Figure 9. Figure 9 shows that the canard plus body configuration has small induced roll moments when compared to the body plus tail configuration. The canards appear to contribute little to the induced roll moments of the canard plus body plus tail configuration. The 15° pitch control deflection of the canards does not appear to influence the induced roll moment of the canard plus body plus tail configuration. The body plus tail and the canard plus body plus tail ($\delta = 0^\circ$) configurations had negative values of $C_{l(4\gamma)}$ at a 5° angle of attack. A small negative value of $C_{l(4\gamma)}$ was shown previously for a Basic Finner configuration at small angles of attack.¹ The stable "lockin" roll trim angle is 45° or a 90° multiple of 45° when $C_{l(4\gamma)}$ is positive and 0° or 90° multiple of 0° when $C_{l(4\gamma)}$ is negative (see Figure 10). Note that $C_{l(4\gamma)}$ is positive and then changes to negative at higher angles of attack for the canard plus body configuration.

POSITIVE INDUCED ROLL MOMENT COEFFICIENT



NEGATIVE INDUCED ROLL MOMENT COEFFICIENT

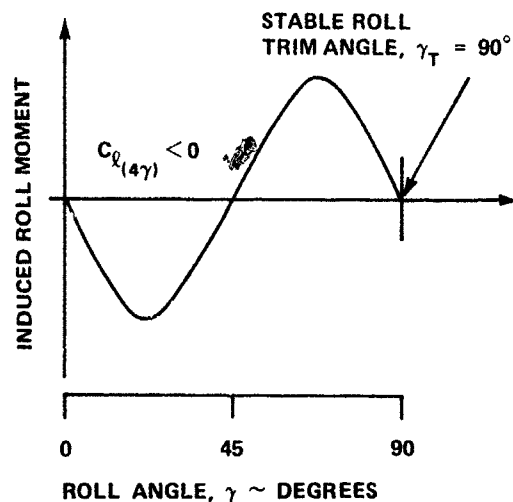
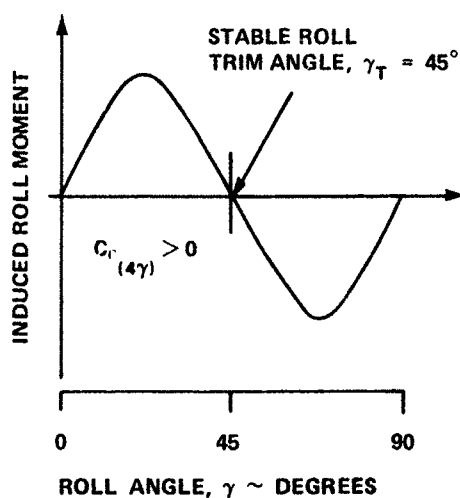
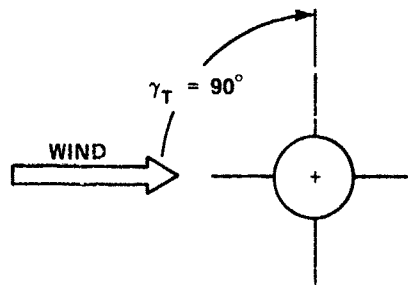


Figure 10. Roll Trim Angle Due to the Induced Roll Moment

Figure 11 presents the extracted fin cant coefficients as a function of angle of attack for the canard-controlled missile configurations. All of the extracted coefficients were small since there was no intentional fin cant.

Figure 12 shows the extracted roll asymmetry moment coefficients versus angles of attack for the canard-controlled missile configurations. The extracted asymmetry roll moment coefficients ($C_{ac} \cos \gamma C_{as} \sin \gamma$) are combinations of mass and aerodynamic asymmetry roll moments. As a result, mass and aerodynamic contributions to the total asymmetry moments cannot be determined unless one of the contributions is known. At zero angle, the aerodynamic asymmetry is "theoretically" zero. Therefore, Figure 12 indicates that the

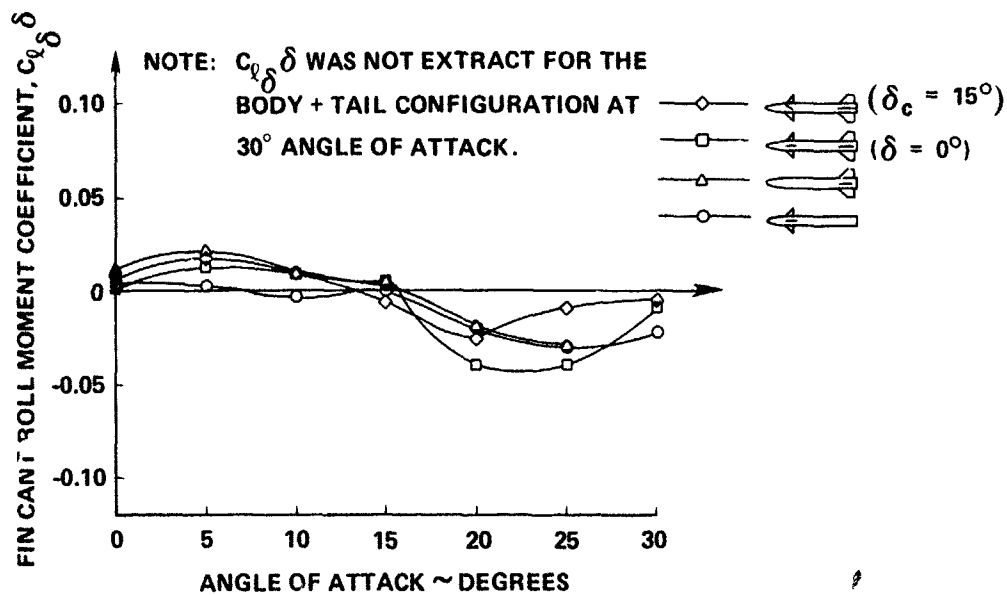


Figure 11. Extracted Fin Cant Roll Moment Coefficients Versus Angle of Attack for Canard-Controlled Missile Configurations

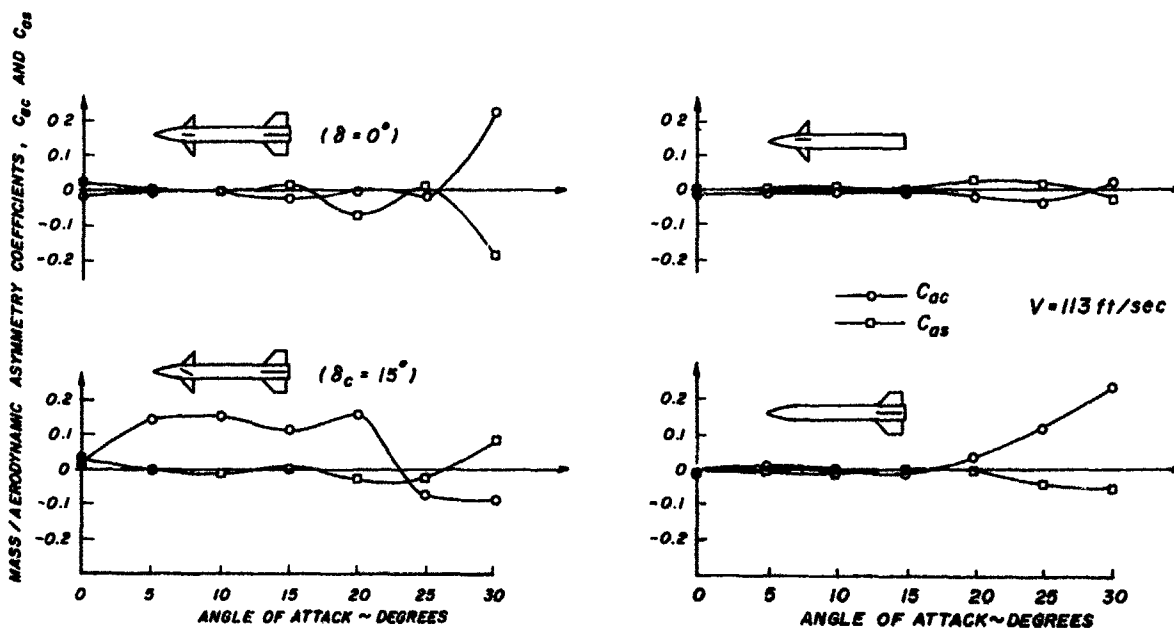


Figure 12. Extracted Mass/Aerodynamic Roll Moment Asymmetry Coefficients Versus Angle of Attack for Canard-Controlled Missile Configurations

mass asymmetries of all the configurations are small. Mass asymmetries are independent of angle of attack and, therefore, constant with angle of attack for each configuration. Thus, the large roll asymmetry coefficients are due primarily to aerodynamic asymmetry moments.

The canard plus body configuration had small asymmetry coefficients and the canard plus body plus tail configuration ($\delta = 15^\circ$) exhibited large aerodynamic asymmetry coefficients that varied as the cosine γ (because of the large asymmetric canard deflections.) These results were anticipated.

However, the symmetric body plus tail and the canard plus body plus tail configurations ($\delta = 0^\circ$) exhibited large aerodynamic roll asymmetries at angles of attack above 25° . The corresponding rolling motion data indicates the presence of a large roll moment that varies as sine γ and/or cosine γ . The origin of these asymmetry type moments is not known.

SUMMARY AND RECOMMENDATIONS

Subsonic free-rolling wind tunnel data have been presented for four canard-controlled missile configurations. Nonlinear static and dynamic roll moment coefficients were extracted from the test data.

Linear roll damping coefficient derivative (C_{ℓ_p}), linear roll damping coefficient derivative variation with roll angle ($C_{\ell_p(4\gamma)}$), induced roll moment coefficient ($C_{\ell(4\gamma)}$), fin cant roll moment coefficient ($C_{\ell\delta}$), and two asymmetry coefficients (C_{ac} and C_{as}) were extracted. The extracted values of these coefficients have been presented for three body build-up configurations (canard plus body, body plus tail, and canard plus body plus tail) with zero fin deflections and a canard plus body plus tail configuration with 15° canard pitch control deflections. The extracted linear roll damping coefficient derivatives (C_{ℓ_p}) were nonlinear with respect to angle of attack for all of the configurations. Extracted experimental values of C_{ℓ_p} for the canard plus

body plus tail configurations ($\delta = 0^\circ$) agreed with predicted values of C_{ℓ_p} up to a 25° angle of attack. The body build-up configurations showed that there is significant canard/tail interference. Because of the canard/tail interference, the body plus tail and the canard plus body plus tail configurations ($\delta = 0^\circ$) have values of C_{ℓ_p} versus angle of attack that are nearly equal. Extracted values of the linear roll damping moment coefficient derivative variation with roll angle ($C_{\ell_p(4\gamma)}$) showed that there is significant roll damping variation with the roll angle for all of the configurations at angles of attack above 25° . The 15° canard pitch control deflections were found to make C_{ℓ_p} more negative at angles of attack greater than 15° . The body build-up configurations also showed that the canards contribute little to the induced roll moment coefficient of the canard plus body plus tail configurations.

The results indicated that the fitting technique and the equation of motion are generally adequate to describe the rolling motion of the canard-controlled missile configurations. However, the large aerodynamic asymmetry coefficients extracted for the symmetry configurations ($20^\circ \leq \alpha \leq 30^\circ$) indicate the presence of aerodynamic moments that are not fully explained by the equation of motion. Future investigations should address this cosine γ /sine γ roll moment phenomena.

Ultimately this technique, if applied to a variety of configurations over a complete Mach number range, could provide a design data base. Transonic and supersonic tests should be included in future efforts. Future work may also include applying Kalman filtering techniques to the fitting technique to streamline the analysis.

APPENDIX A

OBSERVED ROLL ANGLE VERSUS FRAME NUMBER FOR CANARD-CONTROLLED
MISSILE CONFIGURATIONS AT ANGLES OF ATTACK FROM 0 TO 30°

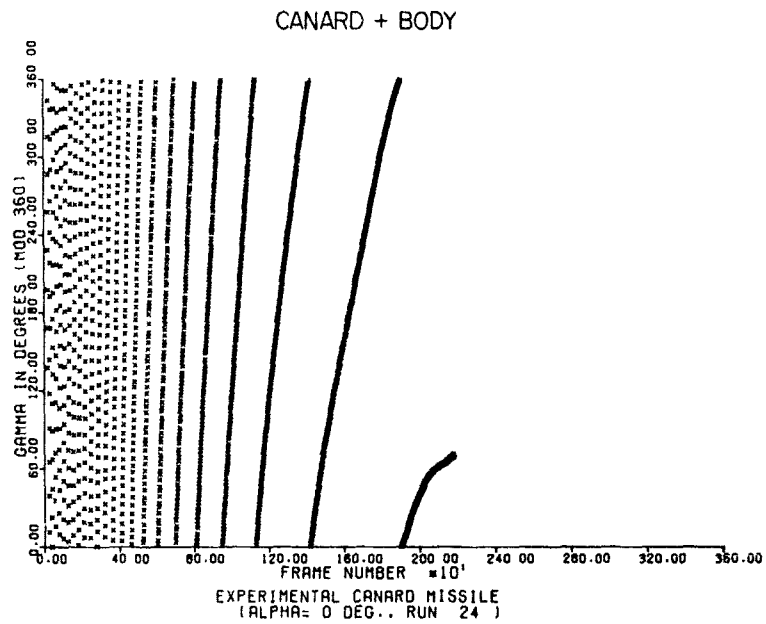


Figure A-1. Observed Roll Angle Versus
Frame Number at a 0° Angle of
Attack for Run 24

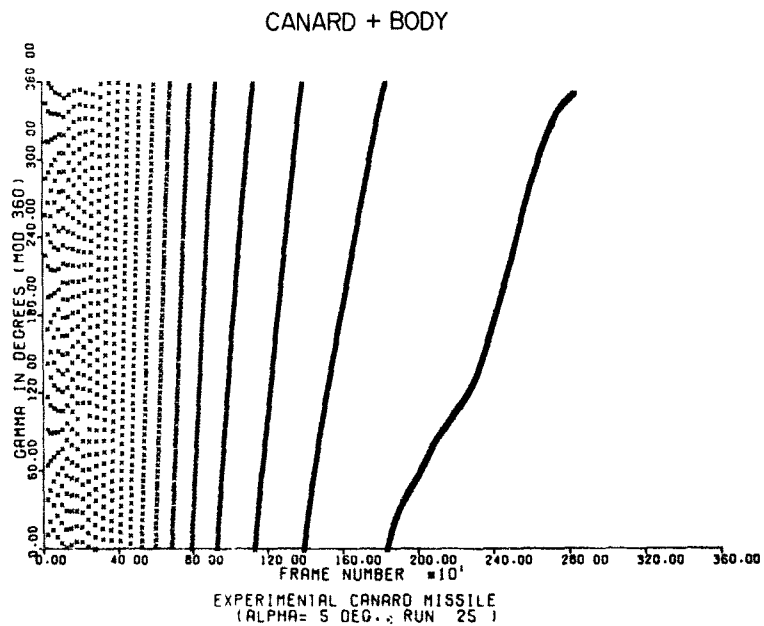


Figure A-2. Observed Roll Angle Versus
Frame Number at a 5° Angle of
Attack for Run 25

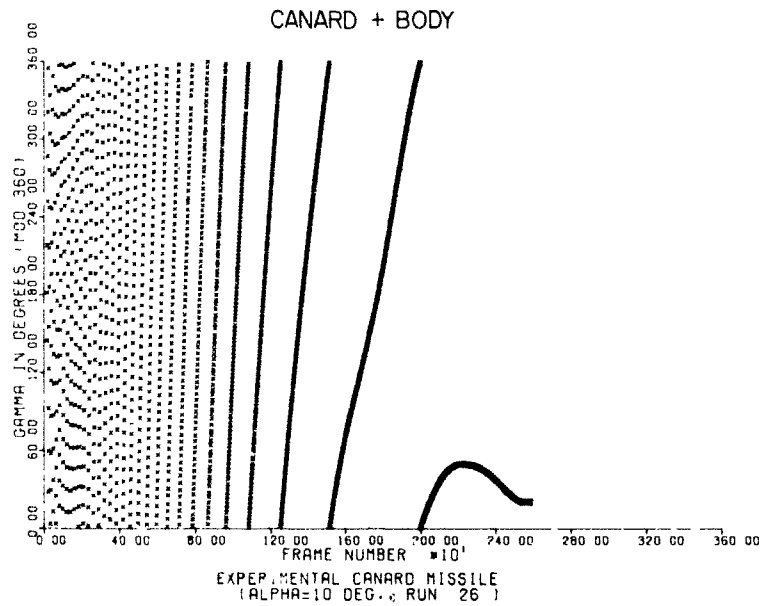


Figure A-3. Observed Roll Angle Versus
Frame Number at a 10° Angle of
Attack for Run 26

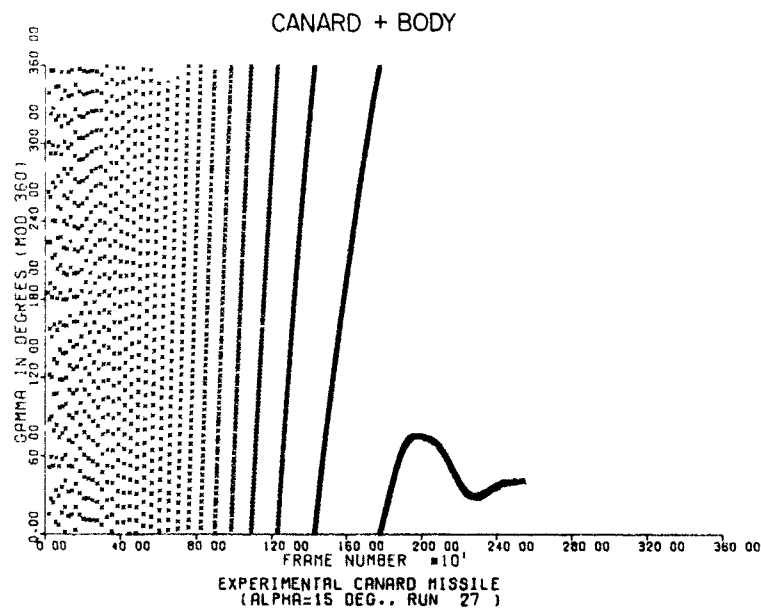


Figure A-4. Observed Roll Angle Versus
Frame Number at a 15° Angle of
Attack for Run 27

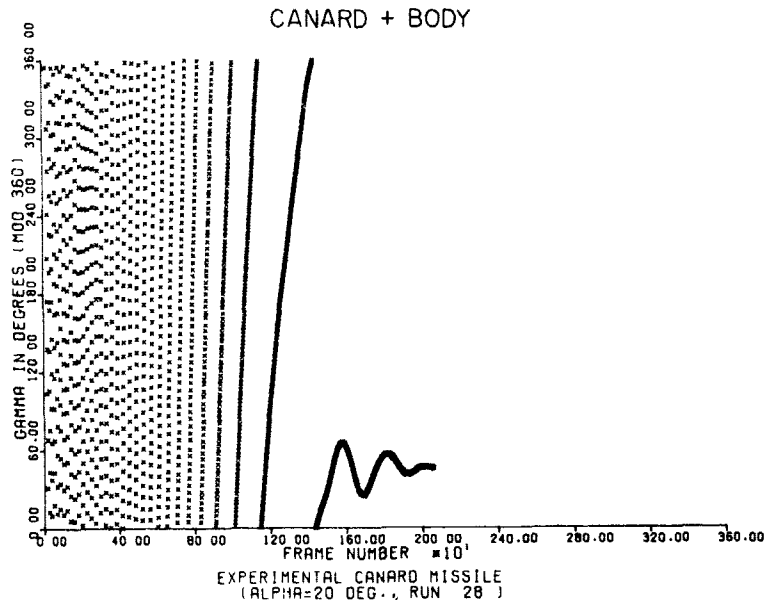


Figure A-5. Observed Roll Angle Versus
Frame Number at a 20° Angle of
Attack for Run 28

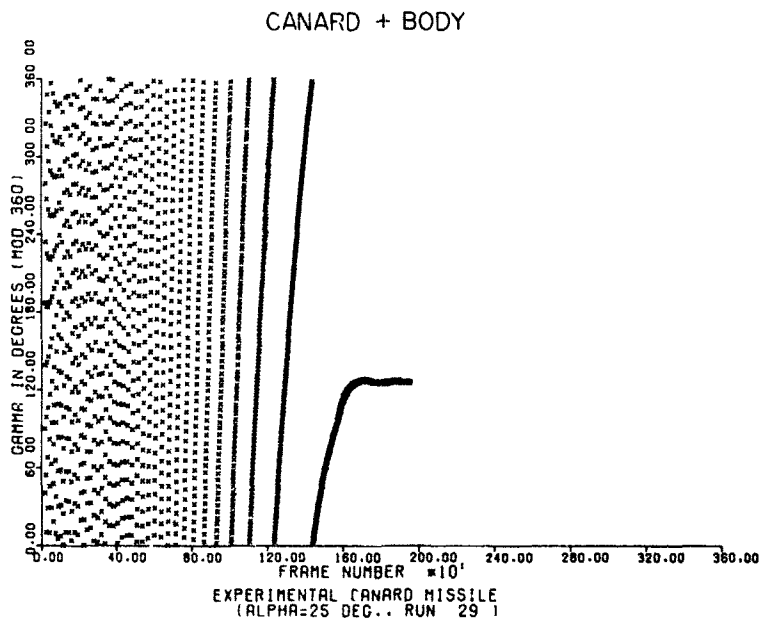


Figure A-6. Observed Roll Angle Versus
Frame Number at a 25° Angle of
Attack for Run 29

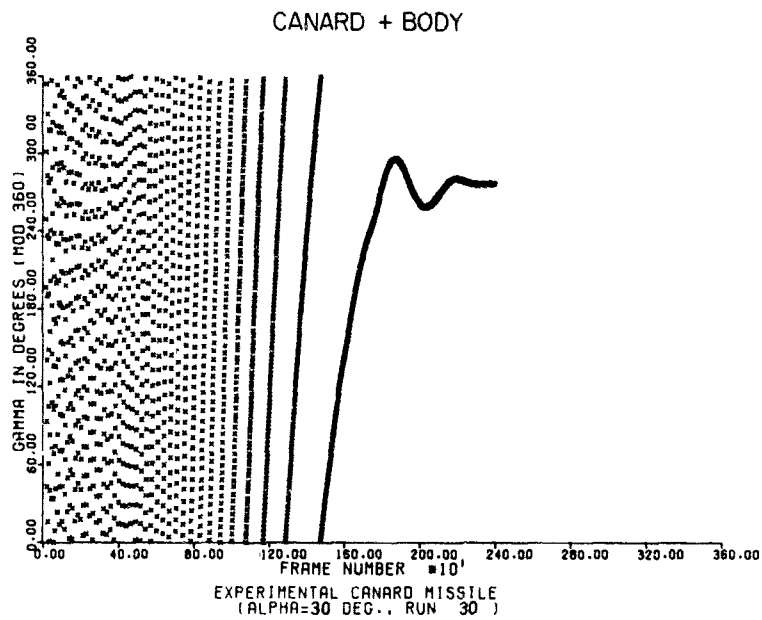


Figure A-7. Observed Roll Angle Versus
Frame Number at a 30° Angle of
Attack for Run 30

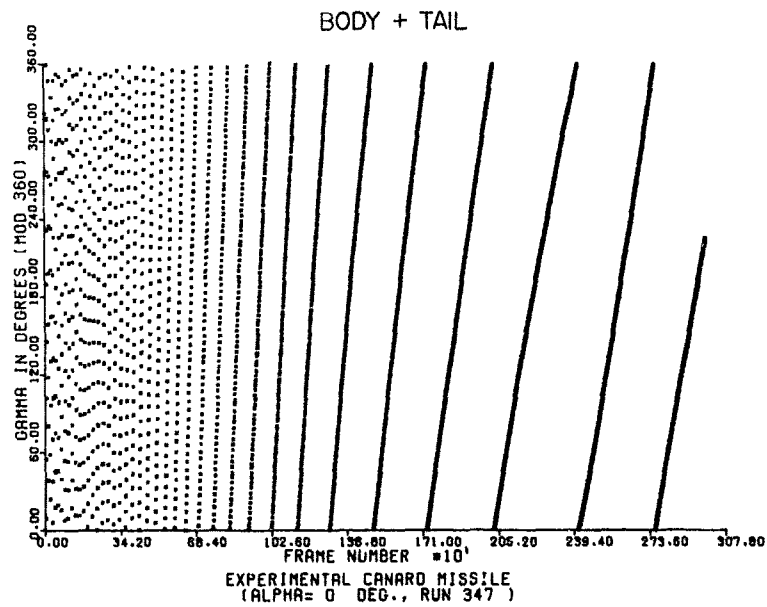


Figure A-8. Observed Roll Angle Versus
Frame Number at a 0° Angle of
Attack for Run 347

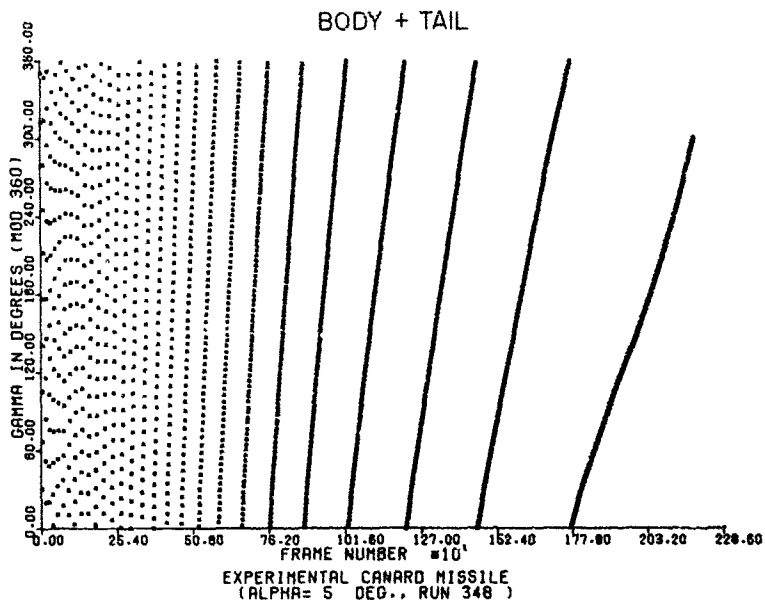


Figure A-9. Observed Roll Angle Versus
Frame Number at a 5° Angle of
Attack for Run 348

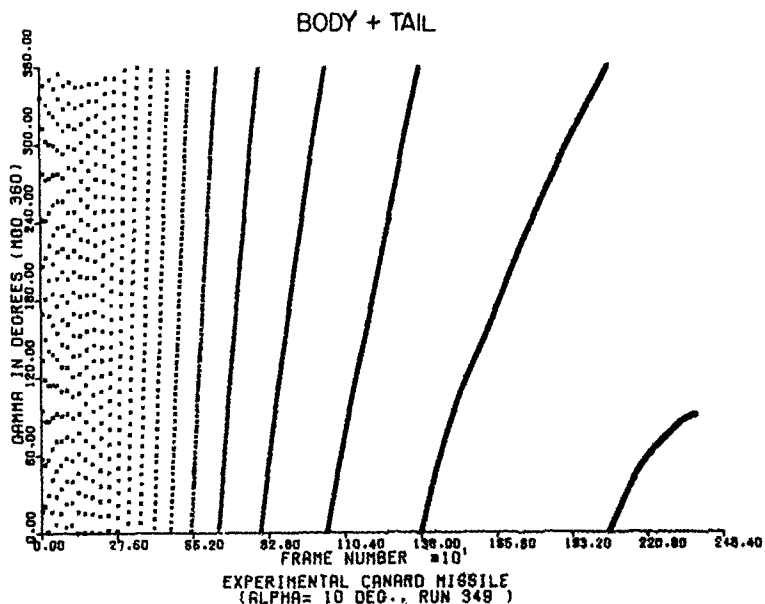


Figure A-10. Observed Roll Angle Versus
Frame Number at a 10° Angle of
Attack for Run 349

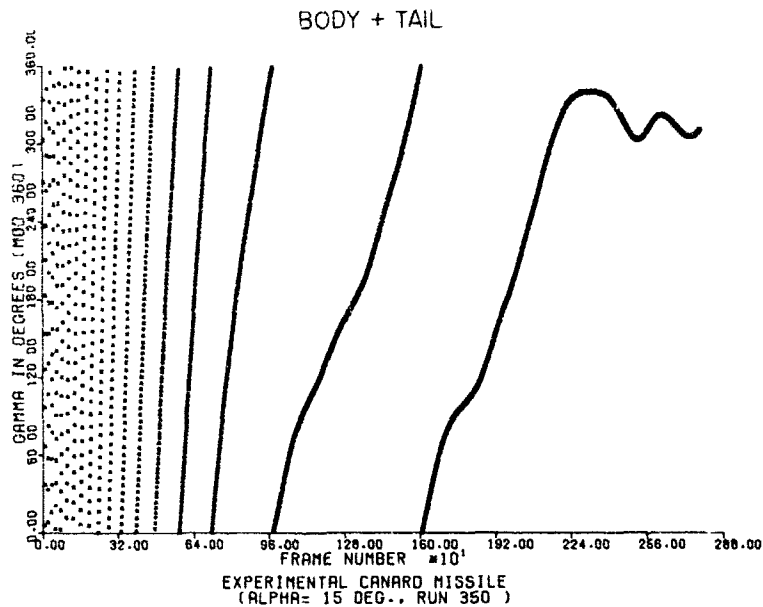


Figure A-11. Observed Roll Angle Versus
Frame Number at a 15° Angle of
Attack for Run 350

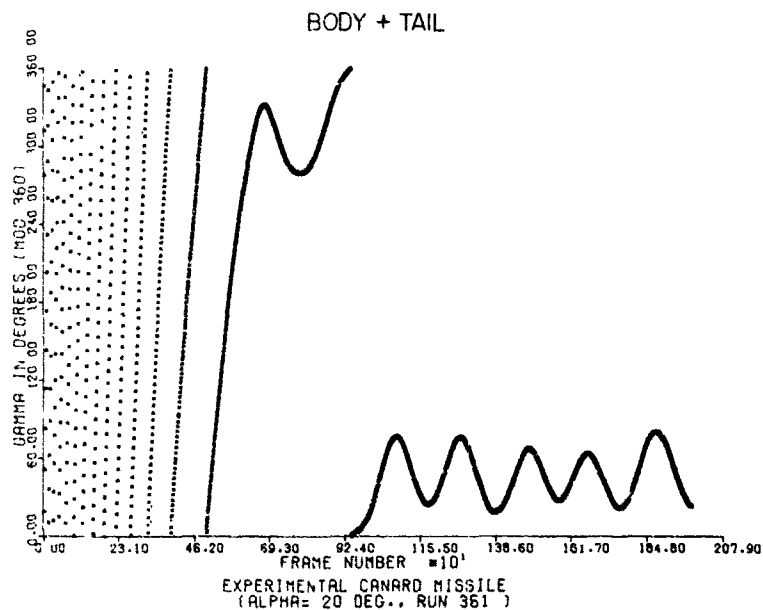


Figure A-12. Observed Roll Angle Versus
Frame Number at a 20° Angle of
Attack for Run 351

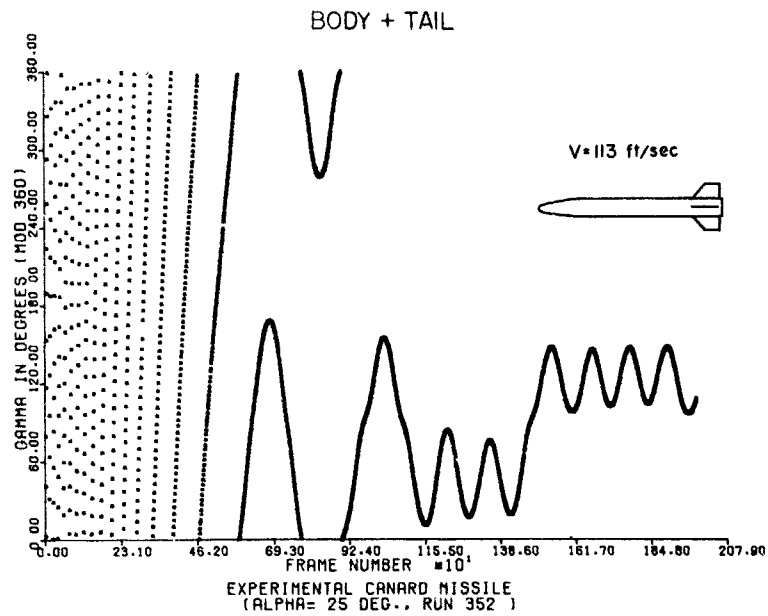


Figure A-13. Observed Roll Angle Versus
Frame Number at a 25° Angle of
Attack for Run 352

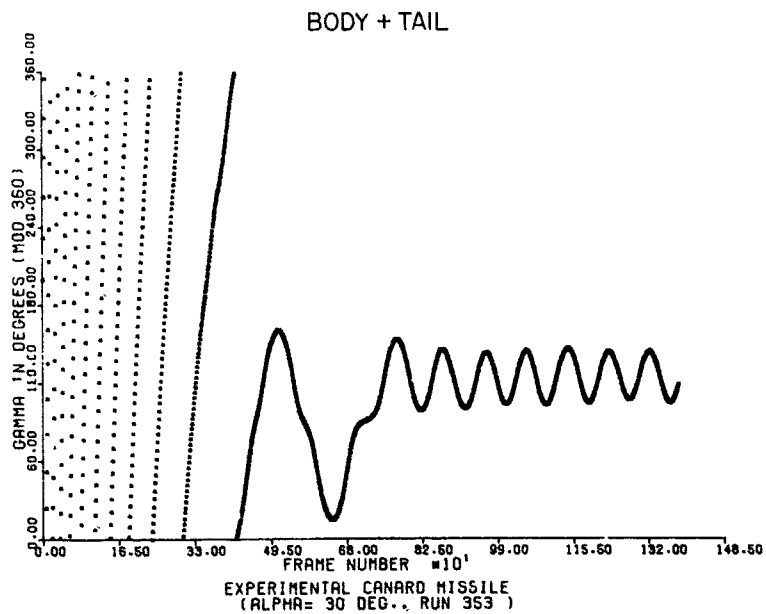


Figure A-14. Observed Roll Angle Versus
Frame Number at a 30° Angle of
Attack for Run 353

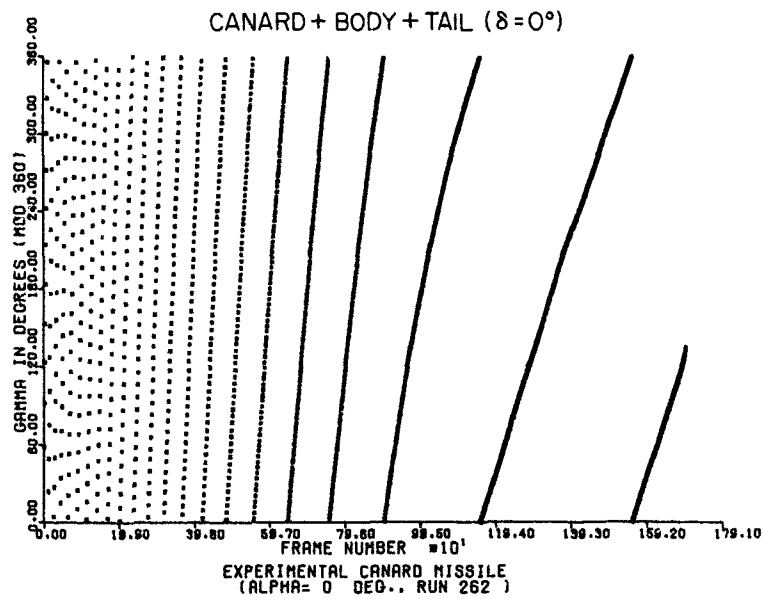


Figure A-15. Observed Roll Angle Versus
Frame Number at a 0° Angle of
Attack for Run 262

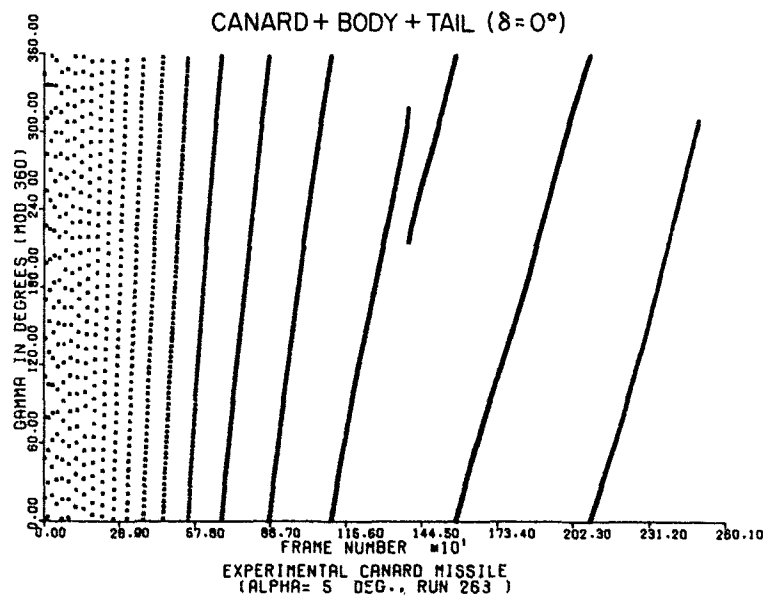


Figure A-16. Observed Roll Angle Versus
Frame Number at a 5° Angle of
Attack for Run 263

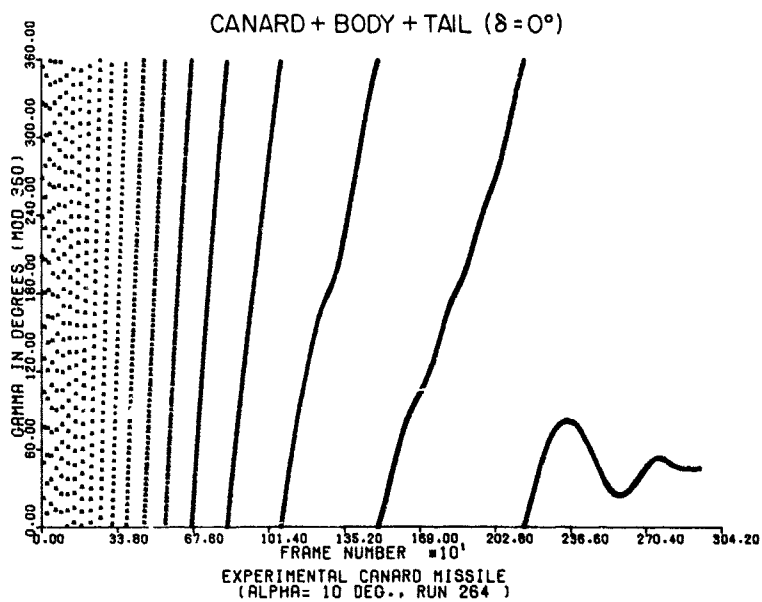


Figure A-17. Observed Roll Angle Versus Frame Number at a 10° Angle of Attack for Run 264

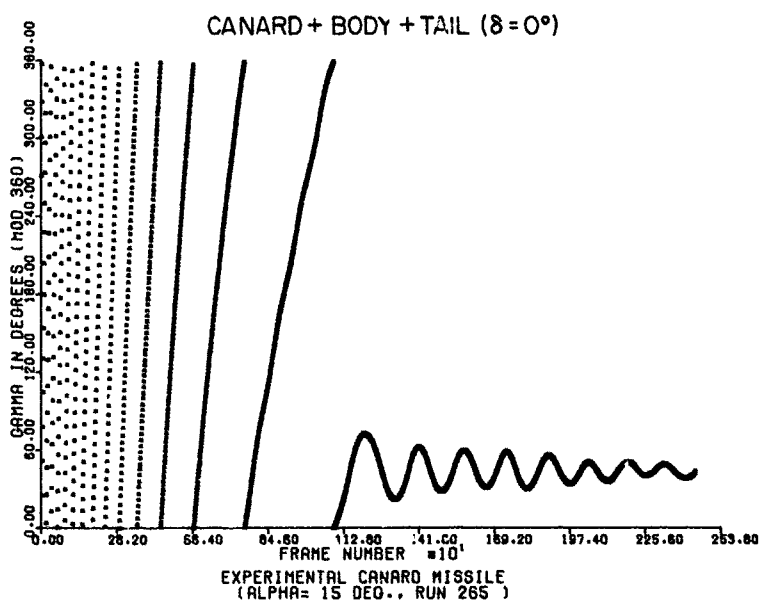


Figure A-18. Observed Roll Angle Versus Frame Number at a 15° Angle of Attack for Run 265

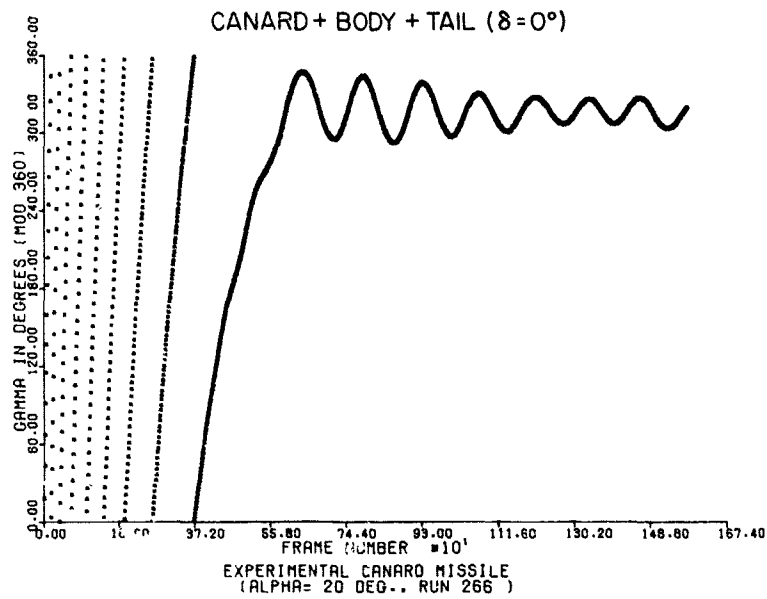


Figure A-19. Observed Roll Angle Versus
Frame Number at a 20° Angle of
Attack for Run 266

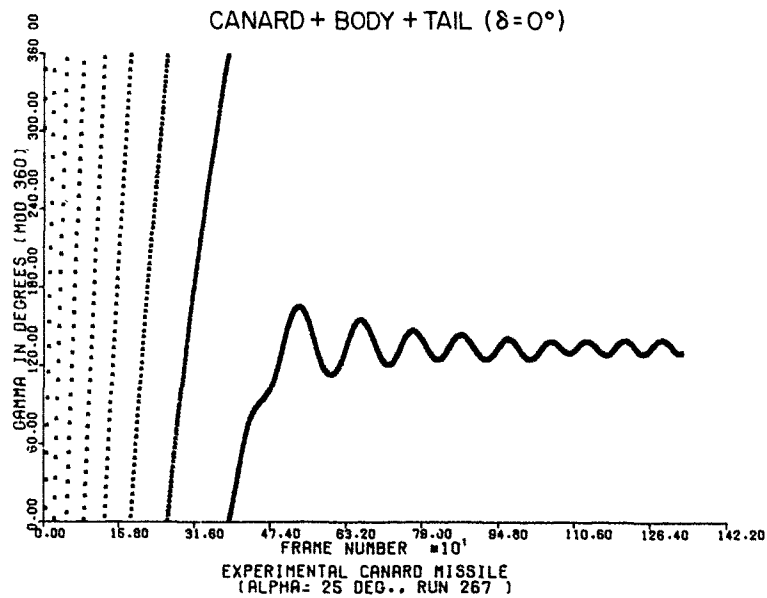


Figure A-20. Observed Roll Angle Versus
Frame Number at a 25° Angle of
Attack for Run 267

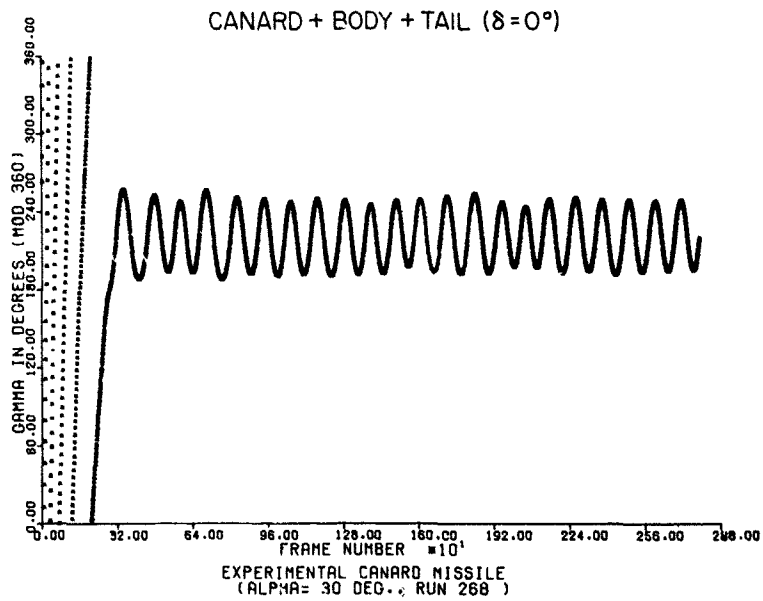


Figure A-21. Observed Roll Angle Versus
Frame Number at a 30° Angle of
Attack for Run 268

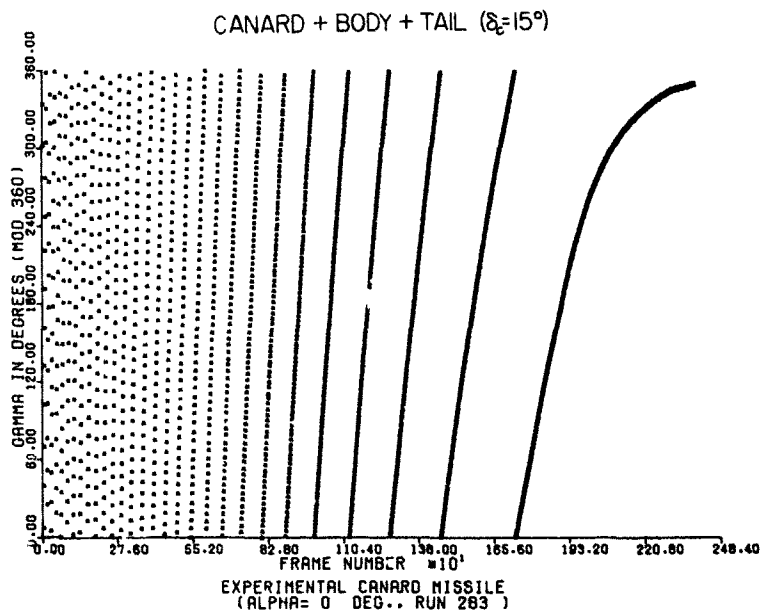


Figure A-22. Observed Roll Angle Versus
Frame Number at a 0° Angle of
Attack for Run 283

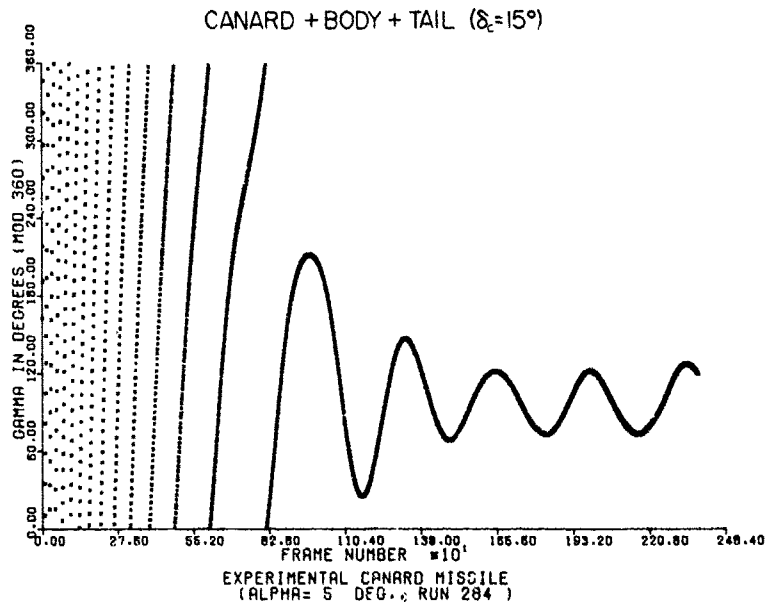


Figure A-23. Observed Roll Angle Versus
Frame Number at a 5° Angle of
Attack for Run 284

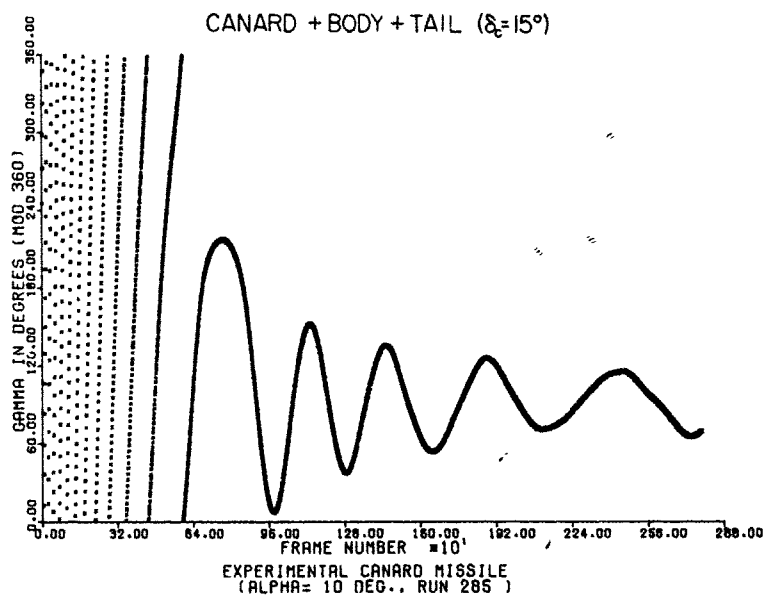


Figure A-24. Observed Roll Angle Versus
Frame Number at a 10° Angle of
Attack for Run 285

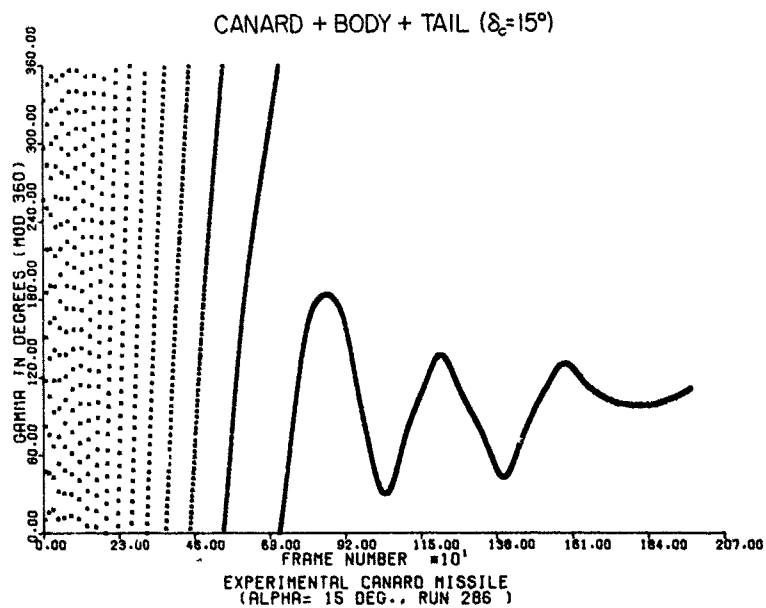


Figure A-25. Observed Roll Angle Versus Frame Number at a 15° Angle of Attack for Run 286

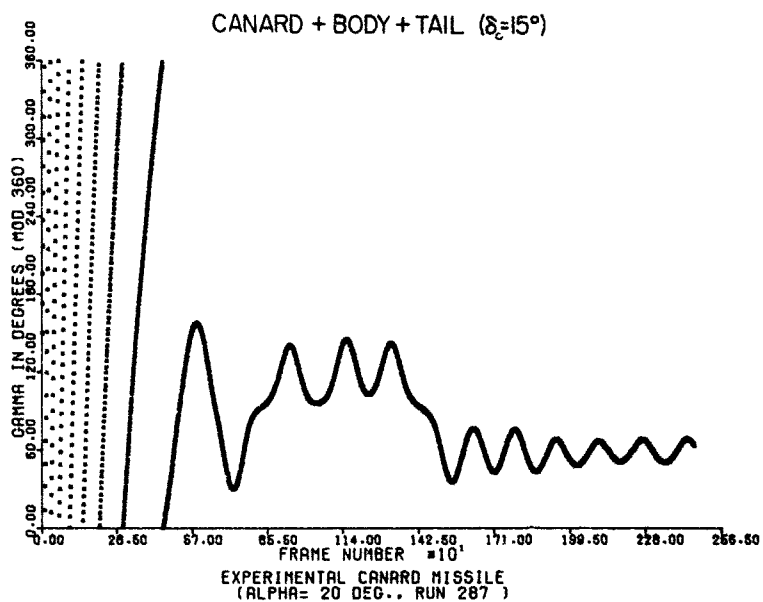


Figure A-26. Observed Roll Angle Versus Frame Number at a 20° Angle of Attack for Run 287

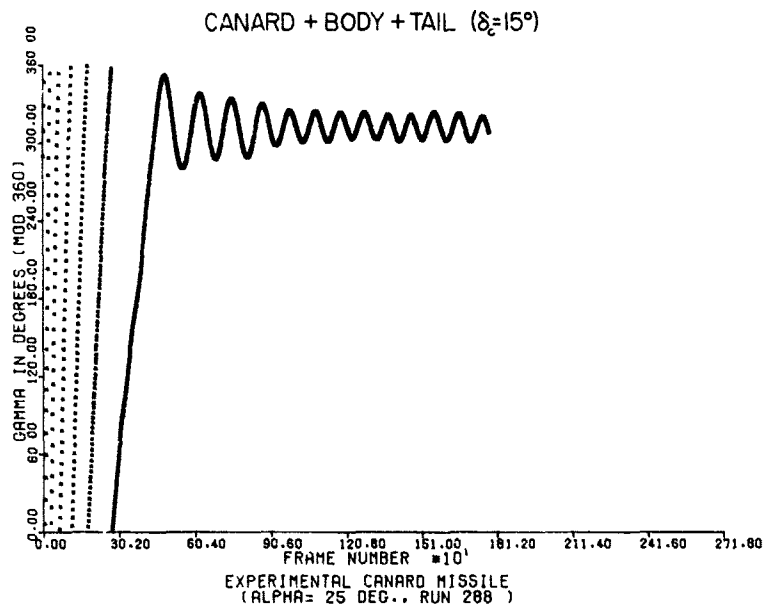


Figure A-27. Observed Roll Angle Versus
Frame Number at a 25° Angle of
Attack for Run 288

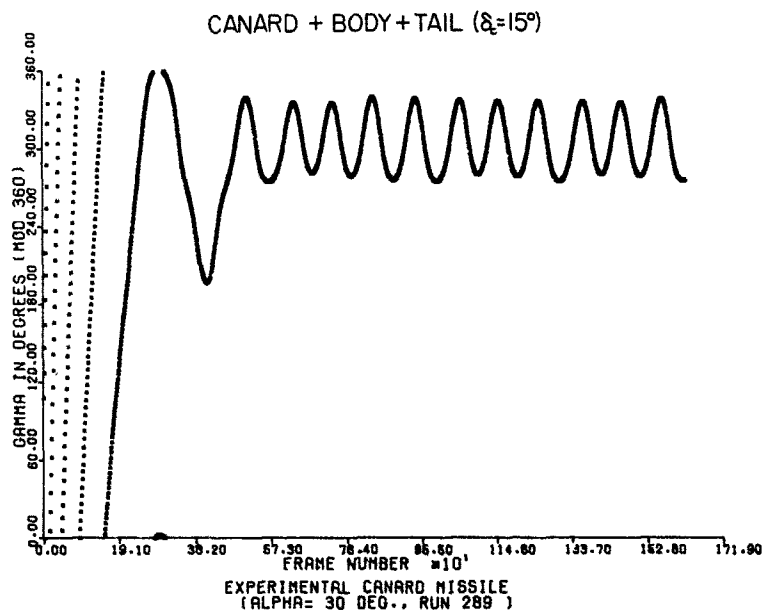


Figure A-28. Observed Roll Angle Versus
Frame Number at a 30° Angle of
Attack for Run 289

APPENDIX B

COMPARISON PLOTS OF COMPUTED AND OBSERVED ROLL ANGLE
VERSUS TIME FOR THE CANARD-CONTROLLED MISSILE
CONFIGURATIONS AT ANGLES OF ATTACK
FROM 0 TO 30°

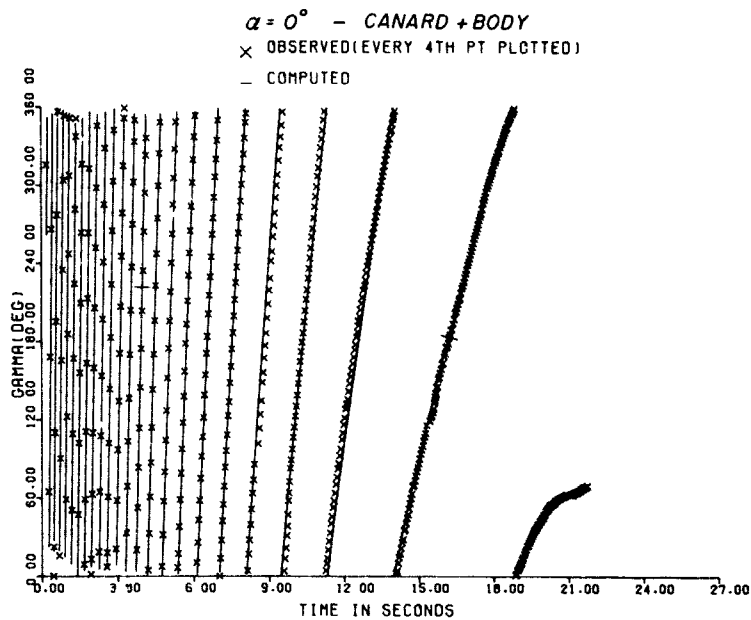


Figure B-1. Comparison of Observed
 and Computed Roll Angles at a 0°
 Angle of Attack for Run 24

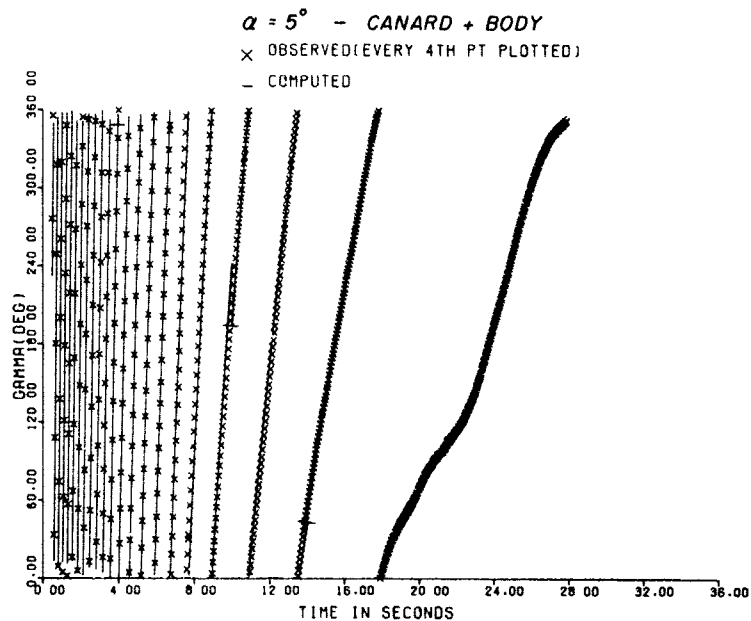


Figure B-2. Comparison of Observed
 and Computed Roll Angles at a 5°
 Angle of Attack for Run 25

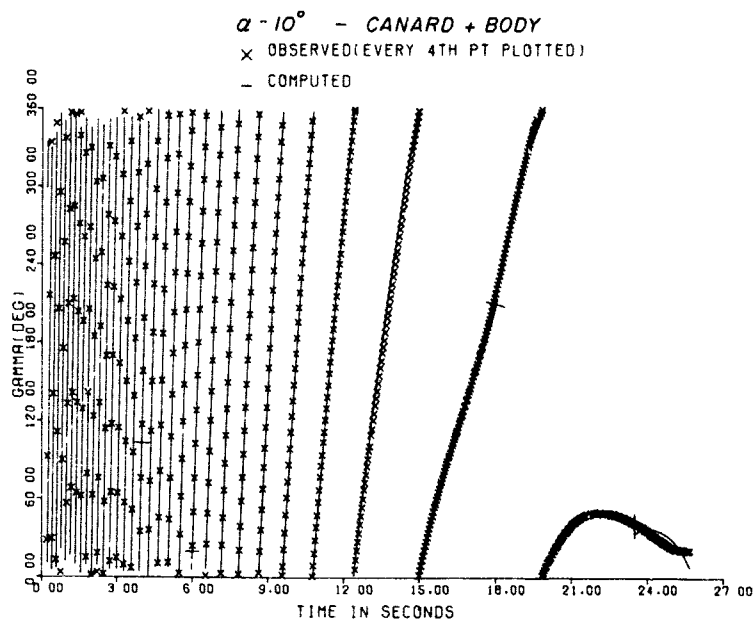


Figure B-3. Comparison of Observed and Computed Roll Angles at a 10° Angle of Attack for Run 26

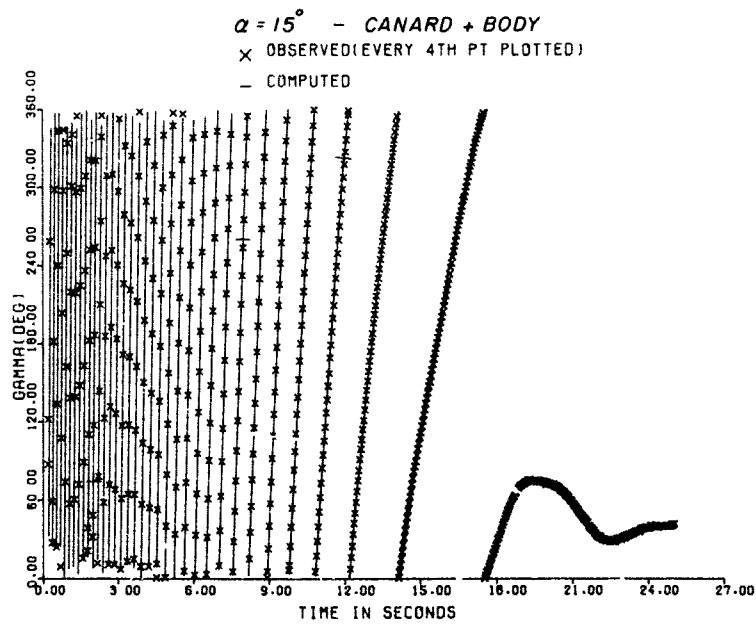


Figure B-4. Comparison of Observed and Computed Roll Angles at a 15° Angle of Attack for Run 27

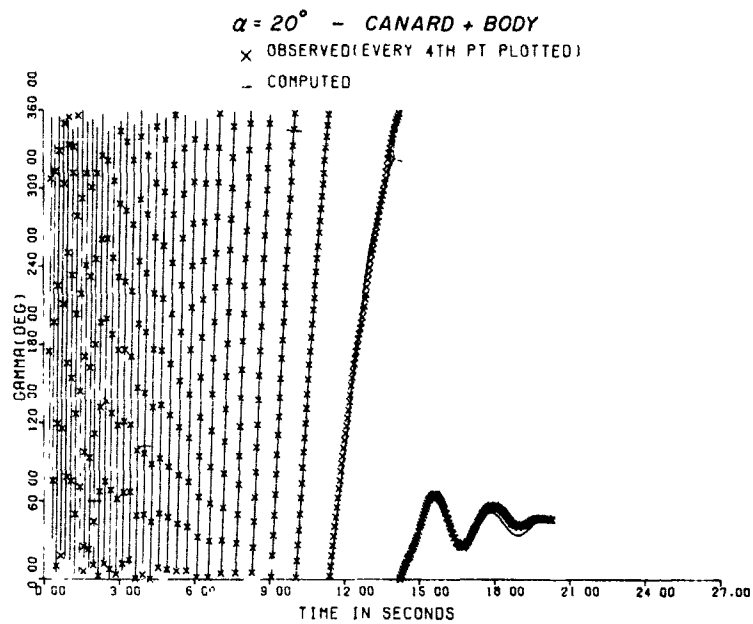


Figure B-5. Comparison of Observed and Computed Roll Angles at a 20° Angle of Attack for Run 28

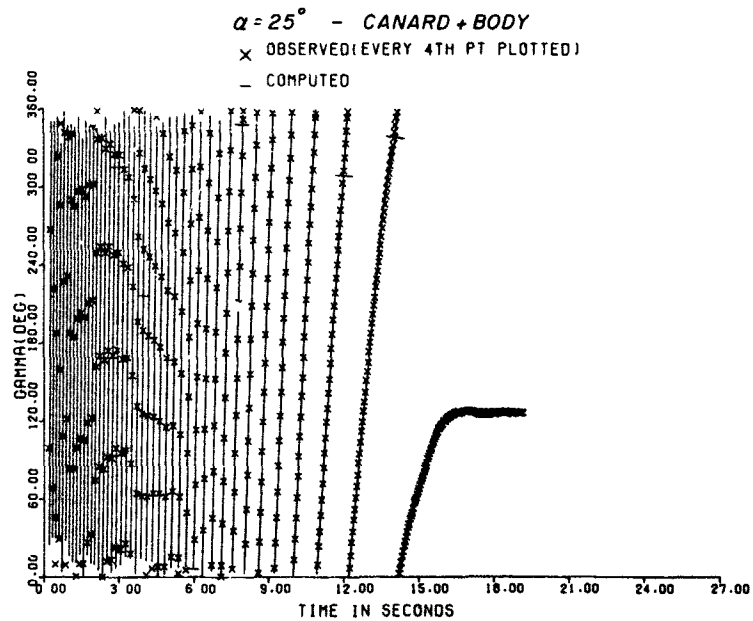


Figure B-6. Comparison of Observed and Computed Roll Angles at a 25° Angle of Attack for Run 29

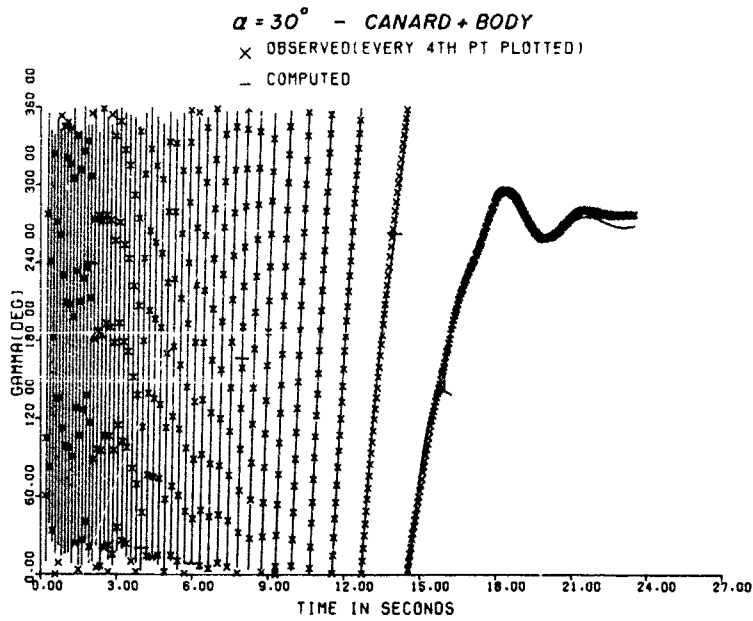


Figure B-7. Comparison of Observed and Computed Roll Angles at a 30° Angle of Attack for Run 30

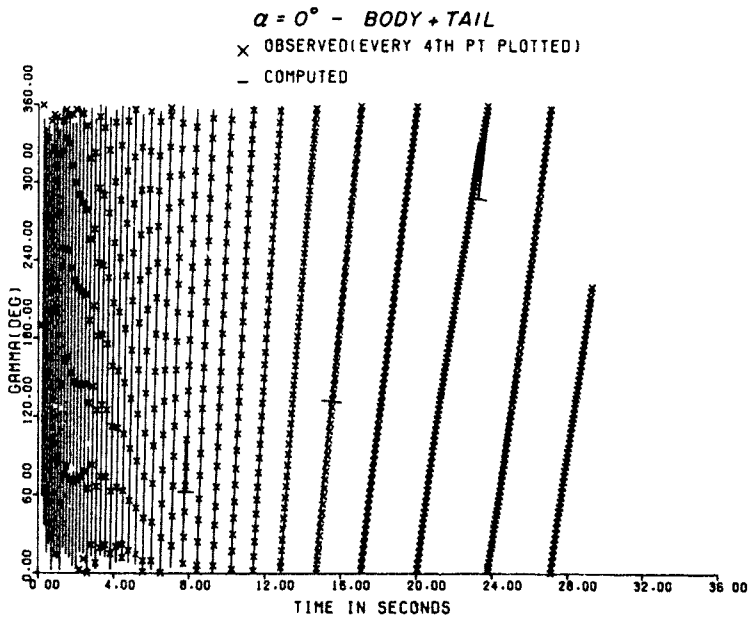


Figure B-8. Comparison of Observed and Computed Roll Angles at a 0° Angle of Attack for Run 347

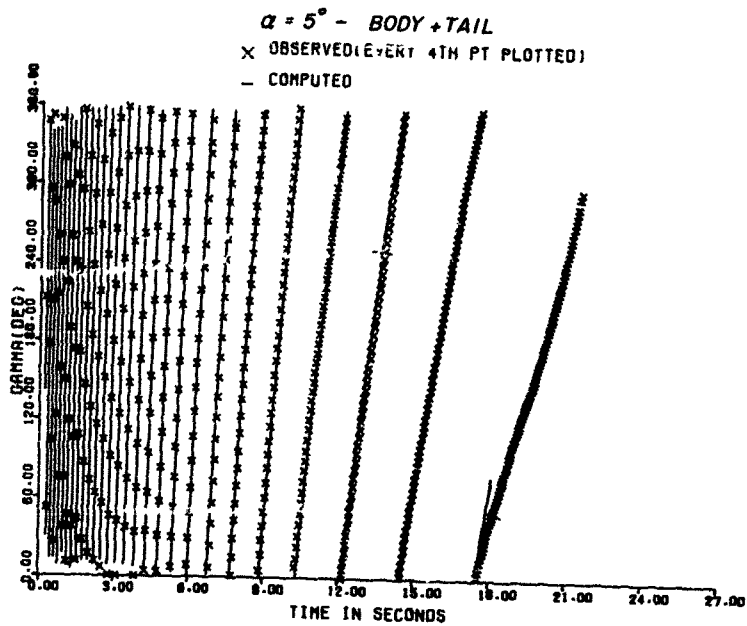


Figure B-9. Comparison of Observed and Computed Roll Angles at a 5° Angle of Attack for Run 348

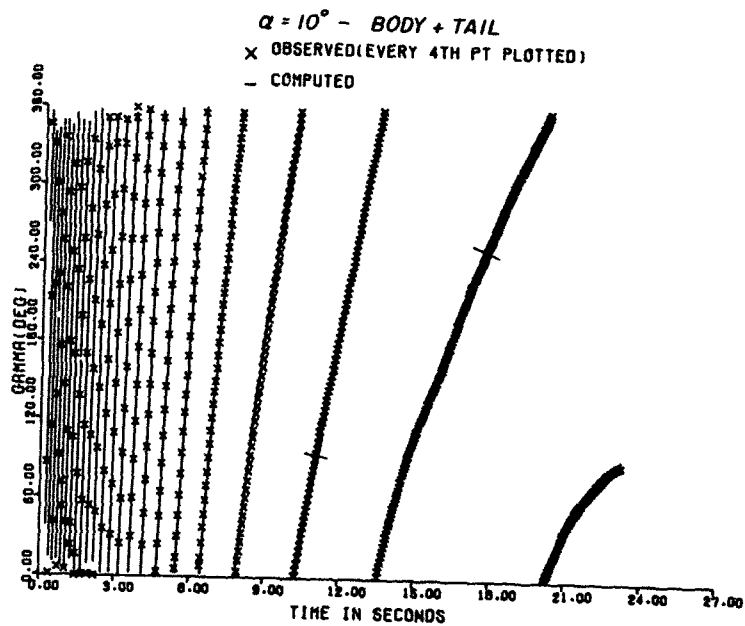


Figure B-10. Comparison of Observed and Computed Roll Angles at a 10° Angle of Attack for Run 349

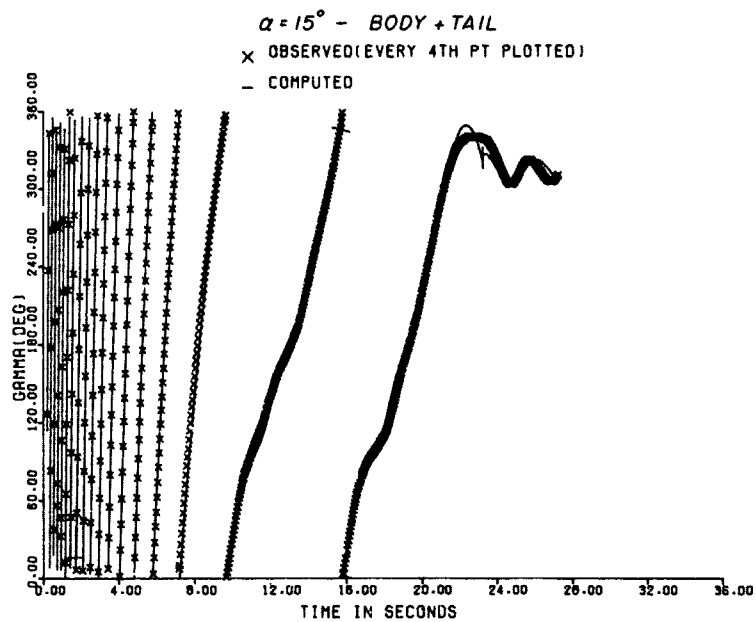


Figure B-11. Comparison of Observed
and Computed Roll Angles at a 15°
Angle of Attack for Run 350

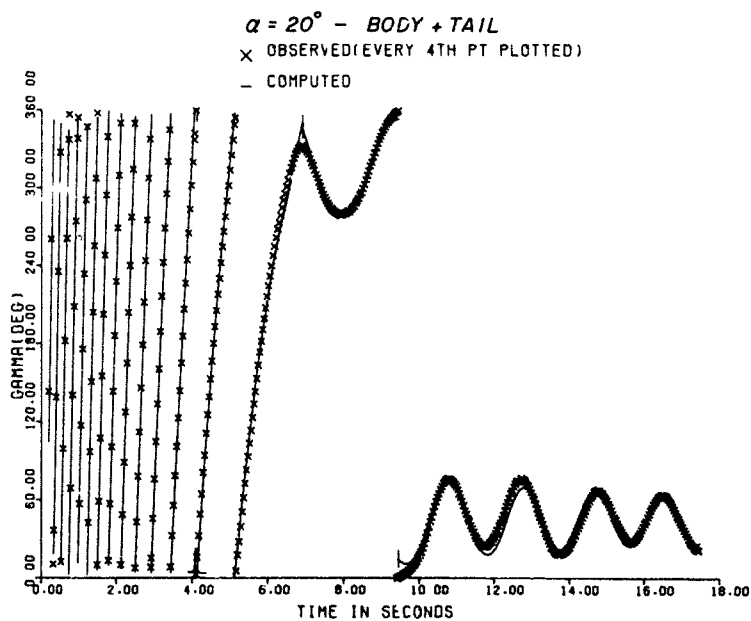


Figure B-12. Comparison of Observed
and Computed Roll Angles at a 20°
Angle of Attack for Run 351

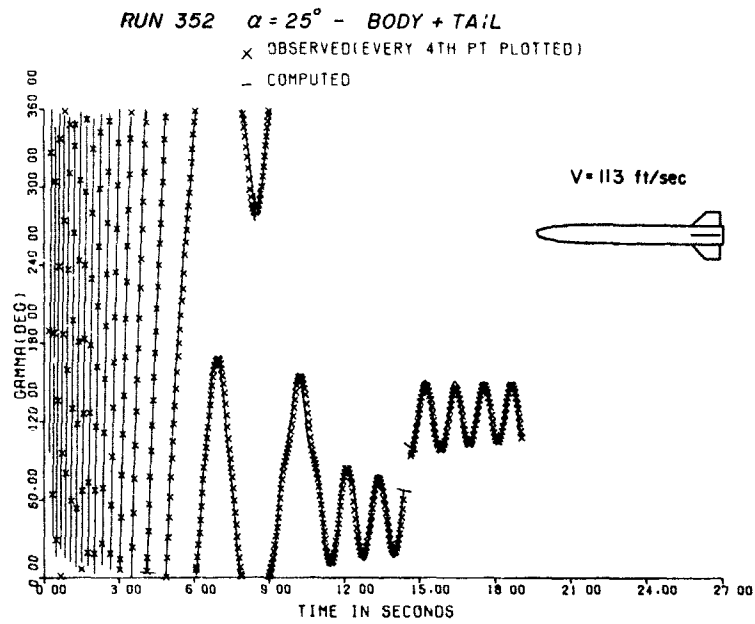


Figure B-13. Comparison of Observed and Computed Roll Angles at a 25° Angle of Attack for Run 352

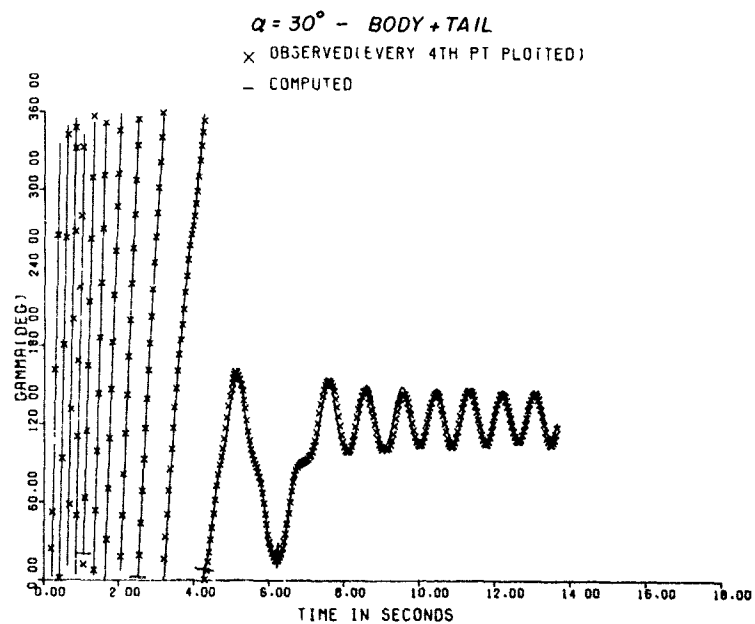


Figure B-14. Comparison of Observed and Computed Roll Angles at a 30° Angle of Attack for Run 353

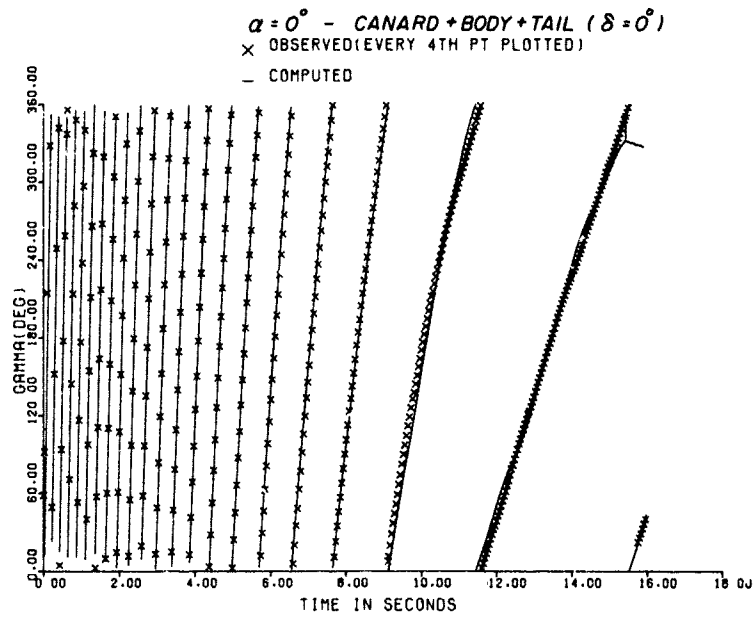


Figure B-15. Comparison of Observed and Computed Roll Angles at a 0° Angle of Attack for Run 262

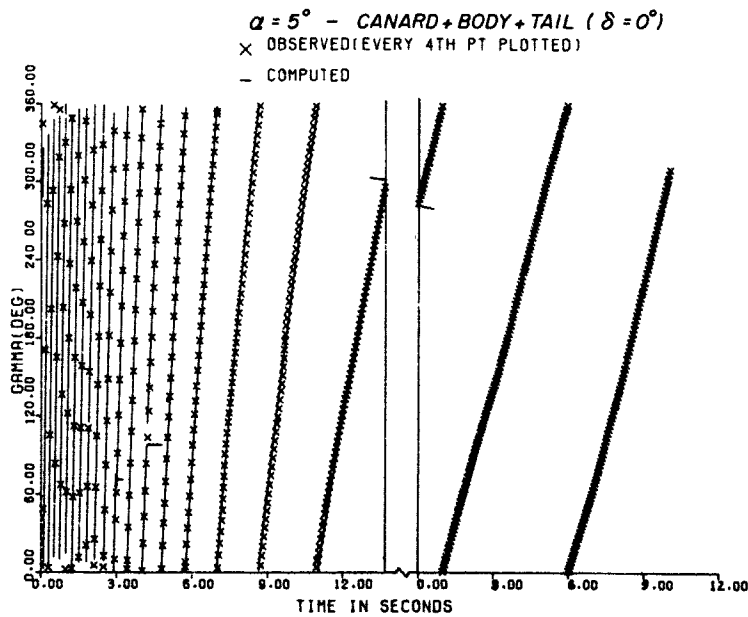


Figure B-16. Comparison of Observed and Computed Roll Angles at a 5° Angle of Attack for Run 263

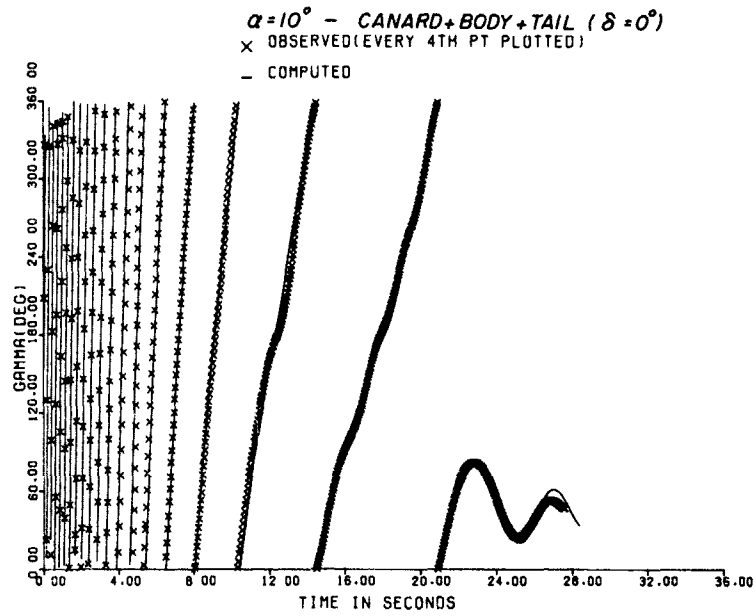


Figure B-17. Comparison of Observed and Computed Roll Angles at a 10° Angle of Attack for Run 264

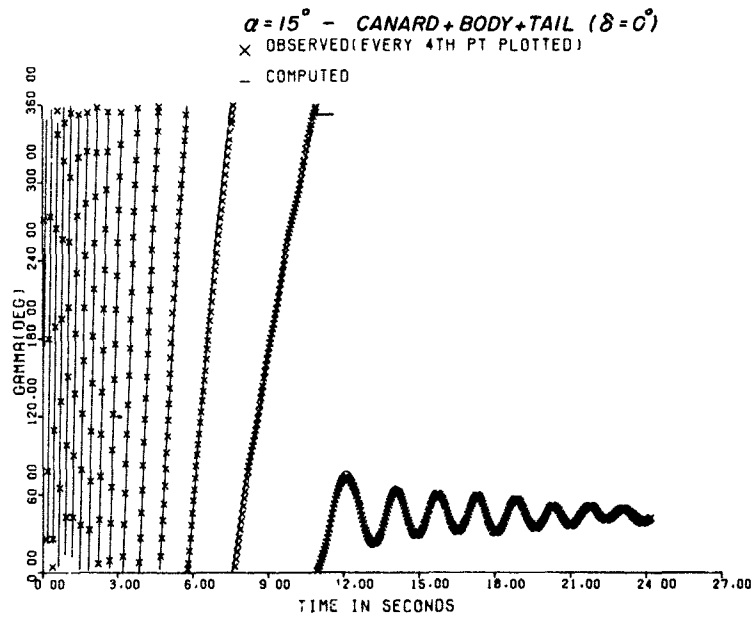


Figure B-18. Comparison of Observed and Computed Roll Angles at a 15° Angle of Attack for Run 265

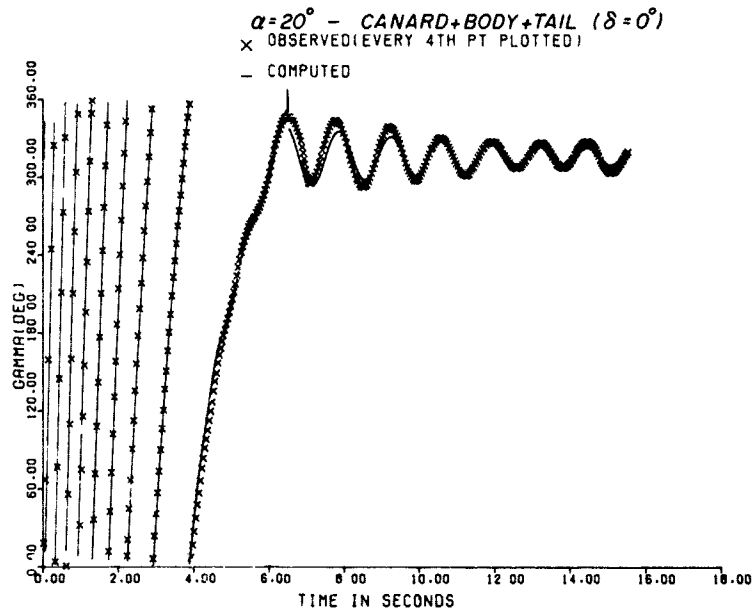


Figure B-19. Comparison of Observed and Computed Roll Angles at a 20° Angle of Attack for Run 266

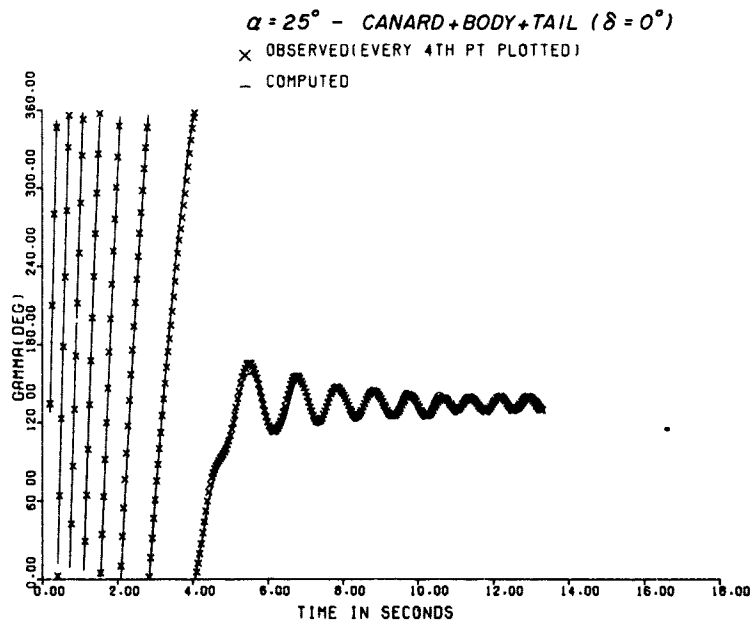


Figure B-20. Comparison of Observed and Computed Roll Angles at a 25° Angle of Attack for Run 267

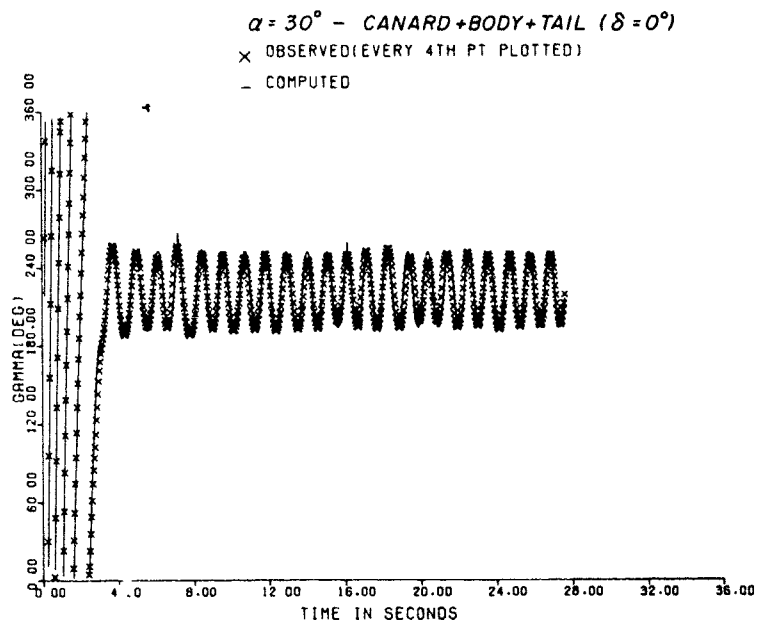


Figure B-21. Comparison of Observed
and Computed Roll Angles at a 30°
Angle of Attack for Run 268

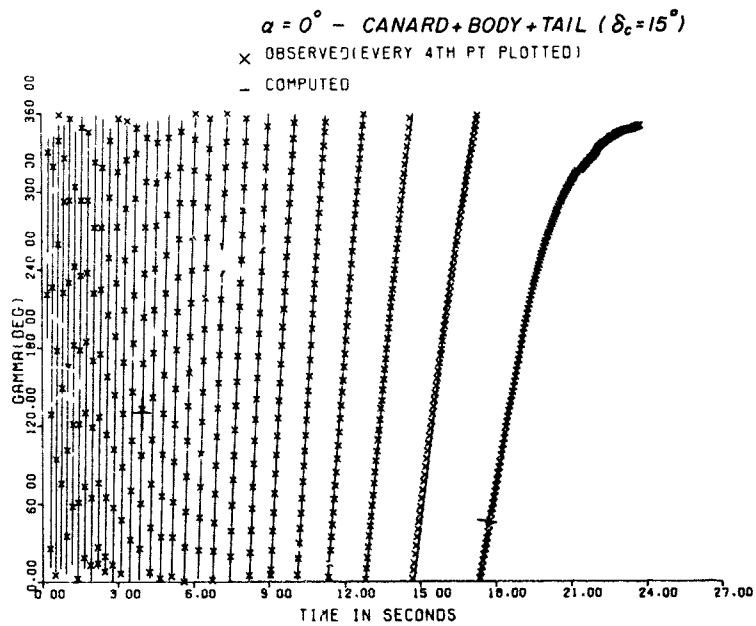


Figure B-22. Comparison of Observed
and Computed Roll Angles at a 0°
Angle of Attack for Run 283

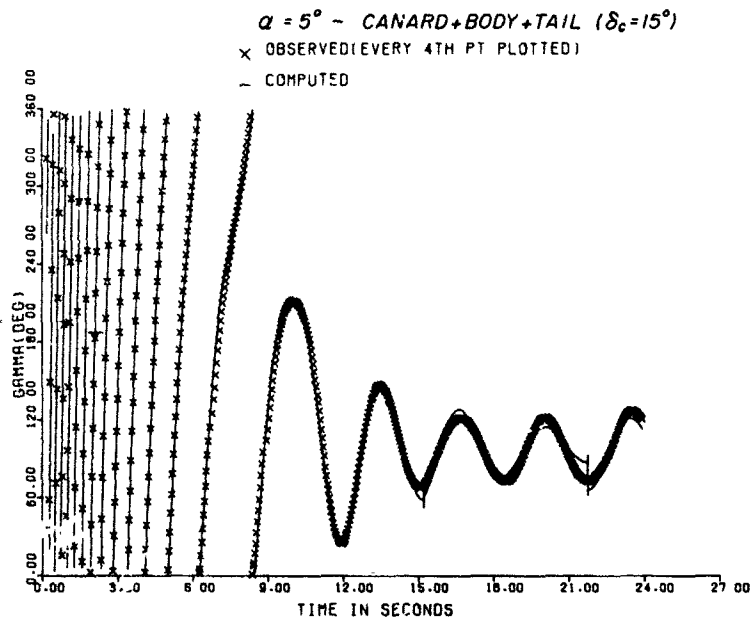


Figure B-23. Comparison of Observed
and Computed Roll Angles at a 5°
Angle of Attack for Run 284

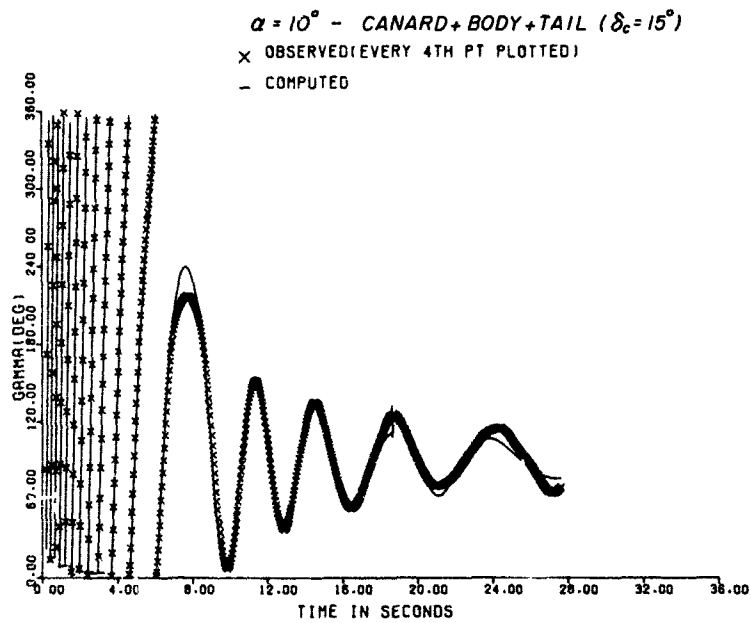


Figure B-24. Comparison of Observed
and Computed Roll Angles at a 10°
Angle of Attack for Run 285

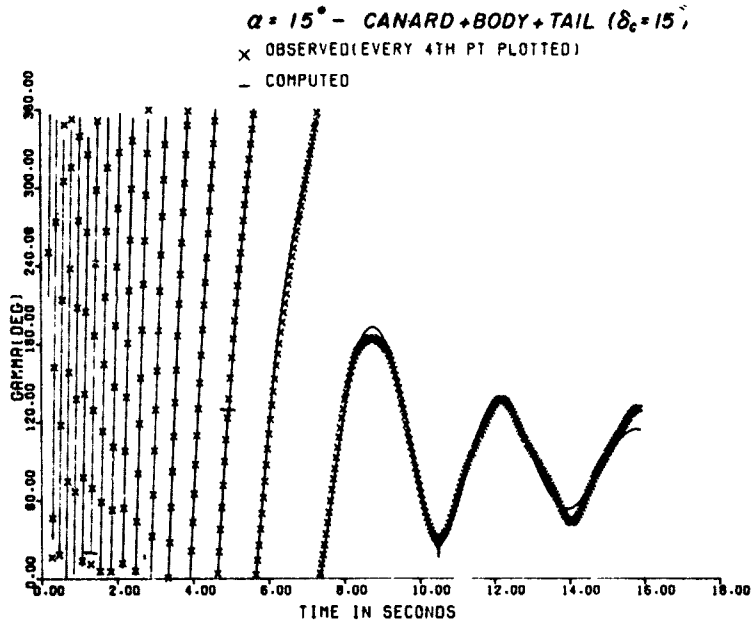


Figure B-25. Comparison of Observed and Computed Roll Angles at a 15° Angle of Attack for Run 286

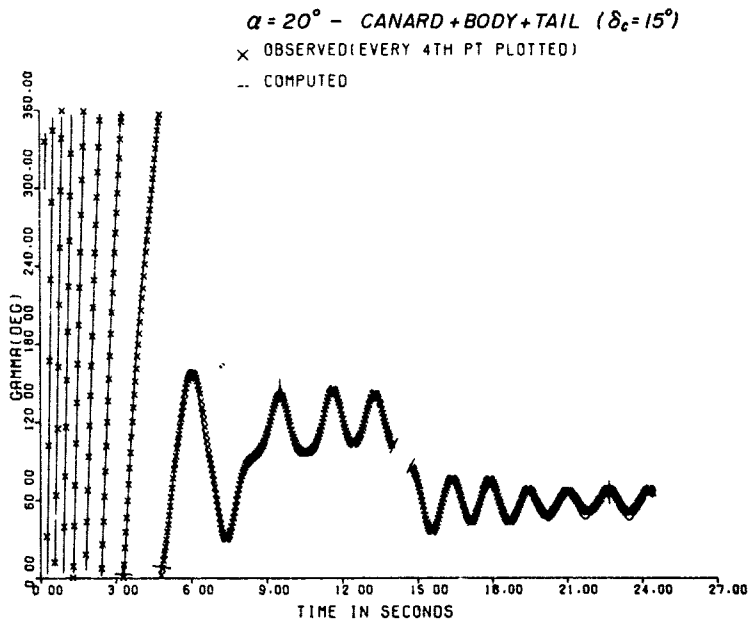


Figure B-26. Comparison of Observed and Computed Roll Angles at a 20° Angle of Attack for Run 287

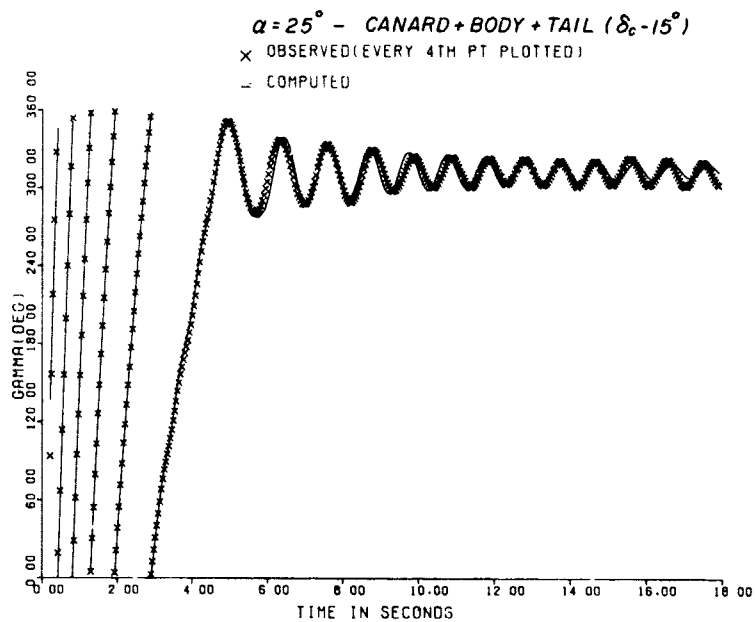


Figure B-27. Comparison of Observed and Computed Roll Angles at a 25° Angle of Attack for Run 288

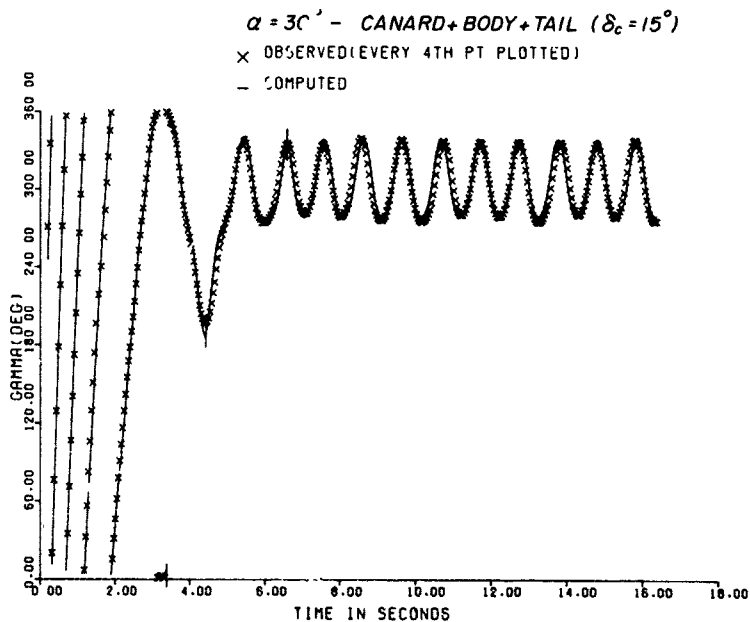


Figure B-28. Comparison of Observed and Computed Roll Angles at a 30° Angle of Attack for Run 289

APPENDIX C
NOMENCLATURE

NOMENCLATURE

C_{as}, C_{ac}	Roll asymmetry coefficients, defined in Equation (1)
C_{jk}, S_{jk}	Roll moment coefficients, defined in Equation (1) (See Table 1)
C_{lp}	Linear roll damping moment coefficient derivative
C_{lpC}	Linear roll damping moment coefficient derivative contribution due to the canards
C_{lpC+T}	Linear roll damping moment coefficient derivative for the canard plus body plus tail configuration ($\delta = 0^\circ$)
C_{lpI}	Linear roll damping moment coefficient derivative due to the interference between the canard and tail
C_{lpj}	j^{th} order roll damping moment coefficient derivative, defined in Equation (1)
$C_{lp(4\gamma)}$	Variation of roll damping moment coefficient derivative with roll angle for a four-finned missile
$C_{lp(4k\gamma)}$	k^{th} variation of roll damping moment coefficient derivative with roll angle for a four-finned missile
$C_{l\delta}$	Fin cant roll moment coefficient
$C_{l\delta(4\gamma)}^\delta$	Variation of fin cant moment coefficient with roll angle for a four-finned missile
$C_{l\delta(4k\gamma)}^\delta$	k^{th} variation of fin cant moment coefficient with roll angle for a four-finned missile

NOMENCLATURE (Continued)

$C_{l_{PT}}$	Linear roll damping moment coefficient for the body plus tail configuration ($\delta = 0^\circ$)
$C_{l(4\gamma)}$	Induced roll moment coefficient for a four-finned missile
$C_{l(4k\gamma)}$	k^{th} induced roll moment coefficient for a four-finned missile
d	Missile reference diameter, $d = 3 \text{ in}$
I_x	Missile axial moment of inertia
p	Missile spin rate, $p = \dot{\gamma}$
Q	Dynamic pressure
$\frac{Q}{I_x}$	$Qs d / I_x$
S	Missile reference area
V	Velocity (ft/sec)
α	Angle of attack
γ	Missile roll angle
$\dot{\gamma}$	Missile roll angular acceleration
δ	Fin deflection angle

NOMENCLATURE (Continued)

($\delta = 0^\circ$)

All fin deflection angles on configuration are zero
(See Figure 1)

($\delta_c = 15^\circ$)

Two opposing canards are deflected 15 to simulate
missile pitch control

DISTRIBUTION

Commander
Naval Air Systems Command
Washington, DC 20360
ATTN: AIR-320, Mr. Bill Volz
Technical Library (2)

Commander
Naval Sea Systems Command
Washington, DC 20360
ATTN: SEA-03, Mr. Lionel Pasiuk
Technical Library (2)

Commander
Naval Material Command
Washington, DC 20360
ATTN: MAT-032, Mr. Sid Jacobson
Technical Library (2)

Commander
Naval Weapons Center
China Lake, CA 93555
ATTN: Code 4063, Mr. Ray Van Aken
Code 4063, Mr. R. E. Meeker
Code 4063, Mr. R. M. Rogers
Technical Library

Army Air Mobility Research and Development Laboratory
Ames Directorate
NASA, Ames Research Center
Moffett Field, CA 94035
ATTN: F. Lazzeroni (Mail Stop N216)
G. Laub (Mail Stop N216)

Commander
Pacific Missile Test Center
Point Mugu, CA 93041
ATTN: Technical Library (2)

Commander
David W. Taylor Naval Ship Research and Development Center
Washington, DC 20007
ATTN: S. Gottlieb
Martin Cook
Technical Library

DISTRIBUTION (Continued)

Chief of Naval Research
Department of the Navy
Washington, DC 20360
ATTN: Technical Library (2)

Superintendent
U.S. Naval Academy
Annapolis, MD 21402
ATTN: Head, Weapons Department
Head, Science Department
Technical Library (2)

Superintendent
U.S. Naval Postgraduate School
Monterey, CA 95076
ATTN: Head, Mechanical Engineering Department
Head, Department of Aeronautics
Technical Library (2)

Officer in Charge
U.S. Naval Scientific and Technical Intelligence Center
U.S. Naval Observatory
Washington, DC 20360
ATTN: Technical Library (2)

Chief of Naval Research
Arlington, VA 22217
ATTN: Mr. Dave Seigel
Technical Library (2)

Chief of Naval Operations
Washington, DC 20350
ATTN: OP-098
Technical Library (2)

Commander
Naval Air Development Center
Warminster, PA 18974
ATTN: Technical Library (2)

Commander
Naval Air Engineering Center
Lakehurst, NJ 19112
Aeronautical Structures Department
ATTN: Aeronautical Structures Department
Technical Library (2)

Approved for Release by NSA on 05-08-2014 pursuant to E.O. 13526

DISTRIBUTION (Continued)

Commanding Officer
Naval Ordnance Station
Indian Head, MD 20640
ATTN: Technical Library (2)

Commandant of the Marine Corps
Headquarters, Marine Corps
Washington, DC 20380
ATTN: Technical Library (2)

Commander
Ballistic Research Laboratory
Aberdeen Proving Ground, MD 21005
ATTN: Dr. C. H. Murphy
Mr. L. McAllister
Dr. A. Platou
Technical Library (2)

Commander
Department of the Army
U.S. Army Armament Research and Development Command
Dover, NJ 07801
ATTN: Mr. A. Loeb
Mr. Mertz
M. Cline
Technical Library (2)

Commander
U.S. Army Missile Command
Redstone Arsenal, AL 35809
ATTN: Mr. Ray Deep (DRSMI)
Dr. D. J. Spring (DRSMI)
Technical Library (2)

Commander
U.S. Army Material Development and Readiness
Command (AMCRD-TP)
5001 Eisenhower Avenue
Alexandria, VA 22304
ATTN: Technical Library (2)

Office of Chief of Research and Development
Washington, DC 20310
ATTN: Technical Library (2)

Commander
Army Chemical Center
Edgewood, MD 21040
ATTN: Technical Library (2)

DISTRIBUTION (Continued)

Commander
Harry Diamond Laboratories
Washington, DC 20013
ATTN: Technical Library (2)

Commanding Officer
U.S. Army Combat Development Command
Field Artillery Agency
Fort Sill, OK 73503
ATTN: President, U.S. Army Field Artillery Board
Marine Corps Liaison Officer
Technical Library (2)

Commanding Officer
Aeronautical Research Laboratory
Wright-Patterson Air Force Base
Dayton, OH 45433
ATTN: Head, Aeronautical System Division
Technical Library (2)

Commanding Officer
USAF Office of Scientific Research
Washington, DC 20330
ATTN: Technical Library (2)

Commanding Officer
Arnold Engineering Development Center
USAF
Tullahoma, TN 37389
ATTN: Dr. J. Uselton
Dr. L. M. Jenke
Dr. W. B. Baker, Jr.
Technical Library (2)

Headquarters, USAF
Systems Command
Andrews Air Force Base, MD 20331
ATTN: Technical Library (2)

Headquarters, USAF
Washington, DC 20330
ATTN: Technical Library (2)

Commanding Officer
Flight Research Center
Edwards Air Force Base, CA 93523
ATTN: Technical Library (2)

DISTRIBUTION (Continued)

North Carolina State University
Department of Mechanical and Aerospace Engineering
Box 5246
Raleigh, NC 27607
ATTN: Prof. F. R. DeJarnette
Technical Library (2)

The University of Tennessee
Space Institute
Tullahoma, TN 37388
ATTN: Dr. J. M. Wu
Technical Library (2)

Applied Physics Laboratory
The Johns Hopkins University
8621 Georgia Avenue
Silver Spring, MD 20910
ATTN: Technical Library (2)

Director
Advanced Research Projects Agency
Department of Defense
Washington, DC 20305
ATTN: Technical Library (2)

Director
Defense Research and Engineering
Department of Defense
Washington, DC 20305
ATTN: Technical Library (2)

Commander
George C. Marshal Flight Center
Huntsville, AL 35804
ATTN: Technical Library (2)

NASA Goddard Space Center
Greenbelt, MD 20771
ATTN: Technical Library (2)

NASA Lewis Research Center
Cleveland, OH 44101
ATTN: Technical Library (2)

NASA
Washington, DC 20546
ATTN: Technical Library (2)

DISTRIBUTION (Continued)

NASA Ames Research Center
Moffett Field, CA 94035
ATTN: Technical Library (2)

McDonnell Douglas Astronautics Company (West)
5301 Bolsa Avenue
Huntington Beach, CA 92647
ATTN: Dr. Jim Zerikos (Mail Station 13-2)

Lockheed Missiles and Space Co., Inc.
P. O. Box 1103, W. Street
Huntsville, AL 35807
ATTN: B. H. Shirley

Lockheed Missiles and Space Co., Inc.
Department 81-10, Bldg. 154
Sunnyvale, CA 94088
ATTN: Dr. Lars E. Erisson

Nielsen Engineering and Research, Inc.
510 Clyde Avenue
Mountain View, CA 94043
ATTN: Dr. Jack Nelson

California Polytechnic Institute
Aeronautical Engineering Department
San Luis Obispo, CA 93407
ATTN: Dr. John D. Nicolaidis

Defense Documentation Center
Cameron Station
Alexandria, VA 22314 (12)

Library of Congress
Washington, DC 20390
ATTN: Gift and Exchange Division (4)

Defense Printing Service
Washington Navy Yard
Washington, DC 20374

Local:

A
E41
G
G04
G23
G41 (Mr. B. Piper)

DISTRIBUTION (Continued)

G41 (Mr. G. Graff)

K

K01

K20

K21 (10)

K50

K80

K81 (Mr. M. V. Krumins)

K82 (Dr. J. Goeller)

K82 (Mr. F. J. Regan)

N

N20

R

R44 (Dr. J. Solomon)

X210 (2)